THE UNIVERSITY OF MICHIGAN

INDUSTRY PROGRAM OF THE COLLEGE OF ENGINEERING

HEAT AND MASS TRANSFER IN CLOSED, VERTICAL, CYLINDERS WITH SMALL INTERNAL HEAT GENERATION AS APPLIED TO HOMOGENEOUS NUCLEAR REACTORS

By

Elayne M. Brower

May, 1958

IP-290

ACKNOWLEDGEMENTS

The author wishes to express her sincere appreciation to Dr. F. G. Hammitt for his encouragement and aid in the use of the digital computer program and to Dr. H. A. Ohlgren for his aid and advice in the initial phase of the problem.

The financial support of the Atomic Power Development Associates over a part of this program is also gratefully acknowledged.

TABLE OF CONTENTS

LIST OF TABLES

LIST OF FIGURES

NOMENCLATURE

c_v	Specific heat of fluid
g	Acceleration due to gravity
k	Thermal conductivity
l, a	Length and radius of tube
N_{u_a}	Nusselt Number based on radius, ha/k
Q_v	Dimensional volumetric heat source
q_v	Non-dimensional volumetric heat source, $\frac{Q_v\, a^6\, \alpha\, g}{\rho\, \nu\, \kappa\, \ell\, c_v}$
R_{a_a}	Rayleigh Number based on radius and maximum temperature differential, $\frac{\alpha\, g\, a^3\, (T_{wall_{min}} - T_{fluid_{max}})}{\nu\, \kappa}$
R, r	Dimensional and non-dimensional radial coordinates
T	Temperature
t	Non-dimensional temperature differential between wall and centerline at any axial position, $\frac{\alpha\, a^4 g\, \Delta T}{\nu\, \kappa\, l}$; subscript o refers to the top of the tube
t_r	Non-dimensional temperature differential between wall and any radial point r
t_w	Non-dimensional temperature differential along wall between bottom and any axial position; t_{w_o} is between bottom and top of tube, i.e. maximum t_w

NOMENCLATURE (CONT'D)

t	Non-dimensional temperature differential between fluid at centerline and wall at bottom, $t + t_w$; $t_o = t_o + t_{w_o} = R_{a_a} \frac{a}{I}$, maximum non-dimensional temperature differential in system.
U,u	Dimensional and non-dimensional axial velocity
X,x	Dimensional and non-dimensional axial coordinates
α	Coefficient of volumetric expansion
β	Non-dimensional core thickness; $1-\beta$ is the non-dimensional boundary layer thickness
δ, γ, $F(\beta)$, $G(\beta)$, $H(\beta,\delta)$	Non-dimensional functions defined in text
κ	Thermal diffusivity, $\frac{k}{\rho c_v}$
ν	Kinematic viscosity
ρ	Density of fluid

INTRODUCTION

At present the interest in the field of homogenous nuclear reactors, both aqueous and liquid metal, is increasing. However, from the standpoint of a complete powerplant based on such a reactor it appears that considerable data would be desirable, and in fact necessary, on the heat transfer characteristics of fissionable fuels in closed vessels. The most useful consideration at the present seems to be a system where the heat is transferred either from a fissionable fuel inside tubes to a coolant surrounding them or from the fuel in the surrounding areas to the coolant in the tubes. In either case, considerable data on the heat transfer characteristics of the heat generating fluid is desirable.

This investigation was undertaken in an effort to promote some further understanding, beyond the original investigation on this subject by Hammitt[1,2], into the natural convection heat and mass transfer characteristics in closed vertical vessels with internal heat generation.

The work is based on the procedure developed by Hammitt and extends the analytical solution to a lower range of the parameter q_v, i.e. a non-dimensional parameter composed of the volumetric heat source, the length to diameter ratio, and various fluid properties. This extention is of particular interest since it appears that the small passage diameters under consideration for various power reactor concepts result in q_v values below those previously studied, even with the very large volumetric heat fluxes anticipated. Although still restricted to fluids with a Prandtl Number of approximately one (aqueous solutions) this

represents a first effort in extending the previous study (References 1 and 2) in the direction of liquid metal fuels. For such fluids the non-dimensional heat source term, q_V, is an order of magnitude lower than that of an aqueous fluid with the same volumetric heat flux and core dimensions. The present study relates to q_V values of the order that might be anticipated in certain liquid metal fuel reactor designs.

REVIEW OF LITERATURE

The work done up to the present in the field of natural convection has covered many geometries. However, until the inception of the homogenous nuclear reactor little interest was taken in closed vessels and more especially in closed vessels containing a fluid with internal heat generation. The approach of Lighthill[3] considers a tubular vessel of moderate length to diameter ratio, with one end closed and the other end open to an infinite reservoir, and a constant wall temperature. In this analytical investigation no internal heat source and no variable wall distribution are considered. Ostrach[4] extended one phase of the work by Lighthill considering a linear axially-varying wall temperature. An analytical study of a vertical closed tube with internal heat source was made by Murgatroyd[5]. In this case the tube considered had a very large length to diameter ratio so that only fully developed flow, i.e. no change in conditions due to axial position, was considered. The end effects not considered here are thought to be of importance in the reactor concept and hence this solution could not be applied directly.

Experimental investigations were carried out by Martin[6] in an attempt to validate the analytical solution of Lighthill. In general, the types of flow regimes were confirmed, but the experimental heat transfer data exceeded the predicted by a factor of approximately 2.

Haas and Langsdon[7] carried on some short experimental work for the Atomic Energy Commission which compared very well with the experimental results of Hammitt[2].

ANALYTICAL APPROACH

The method presented in Reference 2, and upon which this work is based, considers a completely closed tubular vessel with the heat generated in an arbitrary axial distribution of heat source strength and removed through the walls under an arbitrary temperature distribution. Since the heat source term in a power reactor is considerably higher than conventional sources it was assumed that a modified boundary layer solution applied. Lighthill[3] pointed out that internal flow could be expected to fall within one of three regimes depending on a parameter which is proportional to the product of the Rayleigh Number and the radius to length ratio of the tube. These regimes are:

1) Similarity Regime - if the parameter is small, then the temperature and velocity profiles are fully developed and their shapes (not their magnitudes) do not vary with axial position.

2) Boundary-Layer Regime - if the parameter is very large, the boundary layer does not have sufficient extent to grow into the central portion of the tube and thus occupies only a negligible portion of the radial extent of the tube.

3) Intermediate Regime - those cases in which the boundary layer fills a substantial portion of the tube radially but the "fully developed" regime is not attained.

The boundary layer regime, type 2, of Lighthill was extended in References 1 and 2 to include an internal heat source, both ends closed, and an arbitrary wall temperature distribution. This effectively means that the absolute tube dimensions are large, the heat source is strong,

the length to radius ratio of the tube is small, or the thermal diffusivity and kinematic viscosity of the fluid is small. These factors tend to limit the analysis to aqueous solutions, however, it is felt that some of the trends indicated would apply to liquid metals, especially considering the low values of the overall non-dimensional heat source term q_v.

The analytical solution which was developed appears suitable as q_v increases without limit since the boundary layer becomes increasingly thin. However, as q_v decreases, the boundary layer fills as increasing portion of the cross-sectional area of the cylinder so that at a sufficiently low q_v, presumably depending on the wall temperature distribution, the solution loses significance. It is the purpose of this paper to explore the lower range of q_v, below that considered in Reference 2, and to define the limits for this type of solution, i.e. boundary layer type.

To analyse this problem the following assumptions were made:

1. Boundary layer approximations apply, i.e. partial derivatives of quantities normal to the wall are large compared with those parallel to the wall.

2. Inertia forces of fluid are small compared to shear forces.

3. Boundary layer thickness of velocity and temperatures profiles is the same, i.e. Prandtl Number near unity.

Integral equations for the conservation of mass, momentum, and energy were written for each radial disc or element of the cylinder (Figure 1). Velocity and temperature profiles as shown in Figure 2 were

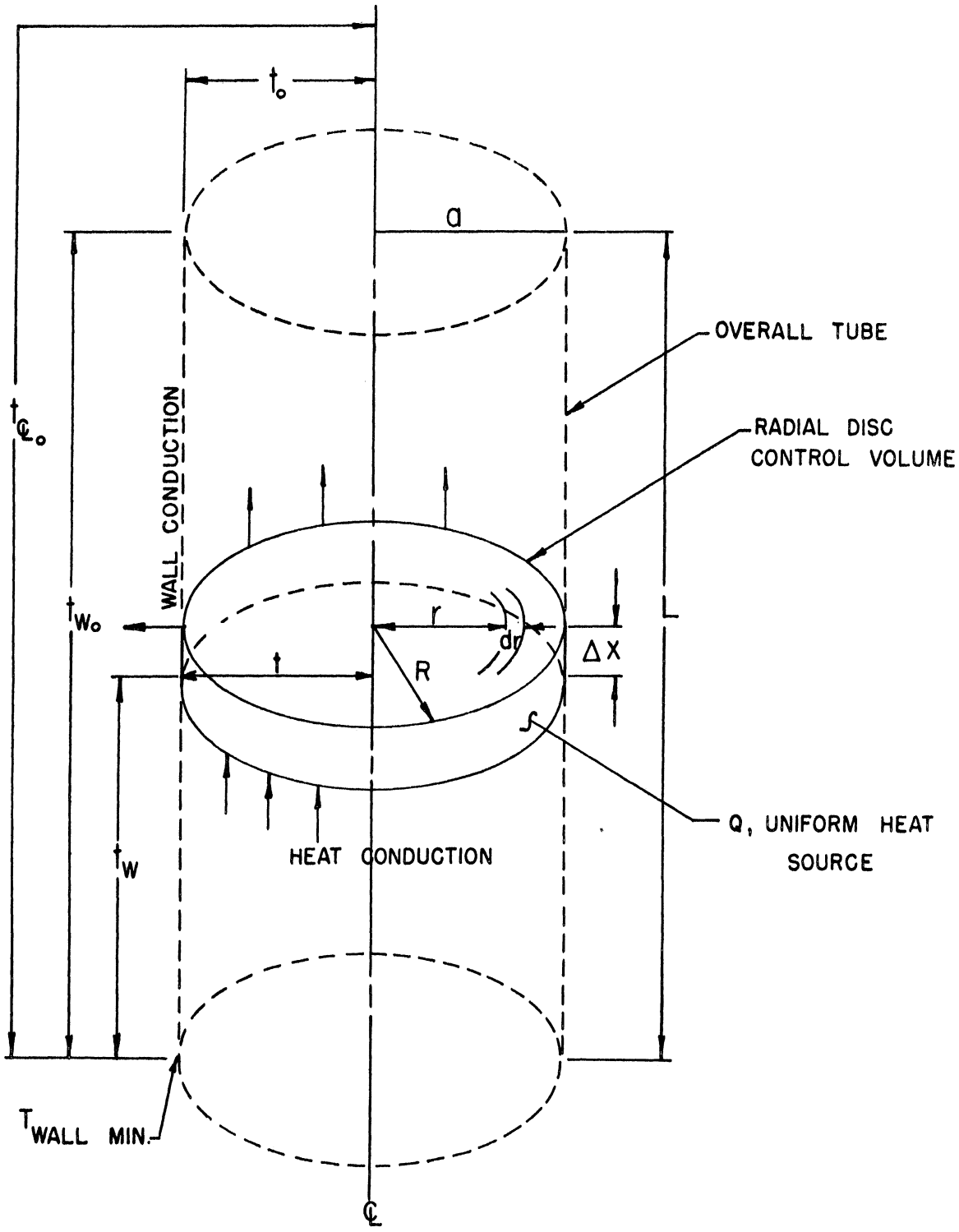

Figure 1. Sketch of Cylindrical Test Section Assumed for Analysis.

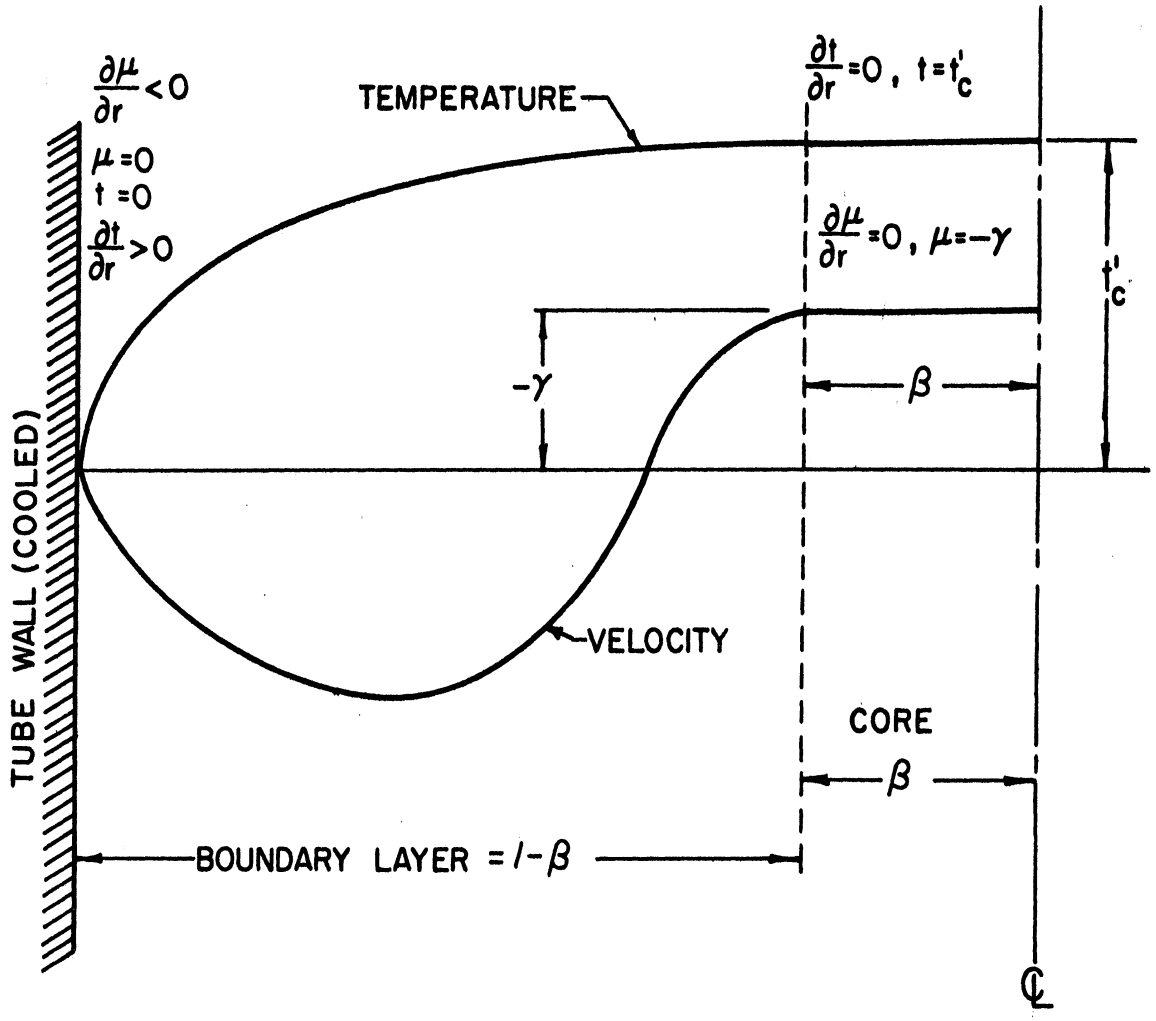

Figure 2. Velocity and Temperature Profiles Assumed in Anaylsis.

assumed and made to satisfy the physical conditions at the wall, centerline, and the boundary layer - core interface for the quantities and their first derivatives.

Hammitt modified these equations to include a volume heat source and an arbitrary wall temperature distribution. Under these conditions the integral equations for the conservation of mass, momentum, and energy are:

$$\int_0^1 r u \, dr = 0 \tag{1}$$

$$\int_0^1 r t \, dr + \frac{1}{2}(t)_{r=0} + \left(\frac{\partial u}{\partial r}\right)_{r=1} = 0 \tag{2}$$

$$\frac{\partial}{\partial x}\int_0^1 r u t \, dr = \left(\frac{\partial t}{\partial r}\right)_{r=1} - \frac{\beta_v}{2} \tag{3}$$

The velocity and temperature profiles following Lighthill are assumed to have the form:

$$u = \begin{cases} -\gamma & 0 < \beta < r \\ -\gamma\left[1 - \left(\frac{r-\beta}{1-\beta}\right)^2 \{1 + \delta(r-1)\}\right] & \beta < r < 1 \end{cases} \tag{4}$$

$$t = \begin{cases} t(x) & 0 < \beta < r \\ t(x)\left[1 - \left(\frac{r-\beta}{1-\beta}\right)^2\right] & \beta < r < 1 \end{cases} \tag{5}$$

Substitution of (4) and (5) into (1) and (2) gives the terms $\delta(\beta)$ and $\gamma(t,\beta)$ as in both the work of Lighthill and Hammitt. The difference between the two analyses evident at this point is that the temperature term, t, is a function of axial distance, x, in Hammitt's case, while it is a constant in Lighthill's work.

The evaluation of the integral energy equation (shown in detail in the Appendix) takes into account the internal heat source term and the variable wall temperature distribution. As can be seen from this derivation the term involving the wall temperature drops out and the equation left is in t only, the temperature between the centerline and the wall as a function of axial position.

$$\frac{d}{dx}\left[t(x)^2 F(\beta)\right] = \frac{t(x)}{1-\beta} - \frac{\varepsilon_r}{4} \qquad (6)$$

Since the equations for the conservation of mass, momentum, and energy have all been used in the development of equation (6) and since there are still two independent variables, t and x, another equation must be developed to permit a solution. This relation (Reference 1) is that between the axial position and the temperature along the centerline of the vessel.

$$\frac{dt(x)}{dx} = \frac{\varepsilon_r}{\gamma} \qquad (7)$$

This is based on the assumption of negligible heat transfer between the ascending core and the decending boundary layer. Putting equation (6) and (7) into a more usable form we have

$$t(x)^2 F(\beta)\Big]_{X_{N-1}}^{X_N} = \int_{X_{N-1}}^{X_N} \frac{t(x)}{1-\beta}\, dx - \int_{X_{N-1}}^{X_N} \frac{q_v}{4}\, dx \qquad (8)$$

$$t(x)\Big]_{X_{N-1}}^{X_N} = \frac{q_v}{\gamma}\left(X_N - X_{N-1}\right) \qquad (9)$$

The temperature term in equation (9) is actually $t_{\mathbb{C}}$ by the nomenclature of Figure 1, where $t_{\mathbb{C}} = t+t_w$, i.e. the temperature from the cylinder centerline to the wall plus the axial variation along the wall from $T_{wall_{min}}$. Hence, equation (9) can be rewritten as

$$t(x) + t_w(x)\Big]_{X_{N-1}}^{X_N} = \frac{q_v}{\gamma}\left(X_N - X_{N-1}\right) \qquad (10)$$

The calculation of these equations was simplified by programming them into an IBM - 650 high speed digital computer. For this purpose equations (8) and (10) were reduced to the approximate difference equations

$$\frac{t_N^2 F_N - t_{N-1}^2 F_{N-1}}{X_N - X_{N-1}} - \frac{t_N + t_{N-1}}{2 - \beta_N - \beta_{N-1}} + \frac{q_v}{4} = \Delta \qquad (11)$$

$$(t+t_w)_N = (t+t_w)_{N-1}\sqrt{1 - \frac{4 q_v (X_N - X_{N-1})}{(t+t_w)_{N-1}^2 (G_N + G_{N-1})}} \qquad (12)$$

For a consistent solution $\Delta \to 0$.

The cylindrical tube was divided into a series of radial discs (Figure 1) and the independent variables could be read into the machine for each disc.

Thus, it was possible to consider arbitrary non-dimensional heat source and non-dimensional wall temperature distributions.

RESULTS

The results for a heat flux range, q_v, from 2×10^9 to 1×10^5 are reported by Hammitt[2]. The work contained herein covers the q_v range from 1×10^4 to a lower limit as defined by the breakdown of the equations and the boundary layer philosophy, i.e. the case where the boundary layer completely fills the tube. At that point a new analysis need be considered and these equations no longer apply. This occurs approximately at a q_v of 5×10^2.

The results in this report are presented in a similar manner to those in Reference 2 since the subject matter is so closely connected.

One of the most significant results is the relation between the non-dimensional temperature, t_{ℓ_o} , and q_v (Figure 3). There is a very slight curvature to these curves over the range 10^9 to 10^2. This is so small, however, that it cannot be detected over the range 10^4 to 10^2 alone or over the range 10^5 to 10^9 alone. Since this curvature is so slight it can be represented by a straight line to a good approximation and the empirical relation

$$q_v = k\, t_{\ell_o}^n$$

developed in Reference 2 is valid. Considering the larger q_v range, from 10^9 to 10^2, more realistic values of the constants k and n can now be determined. These are listed below:

t_{ℓ_o}/t_o	k	n
1.0	0.921	1.22
3.0	0.314	1.24
10.0	0.0791	1.24
20.0	0.0357	1.25
40.0	0.0172	1.25

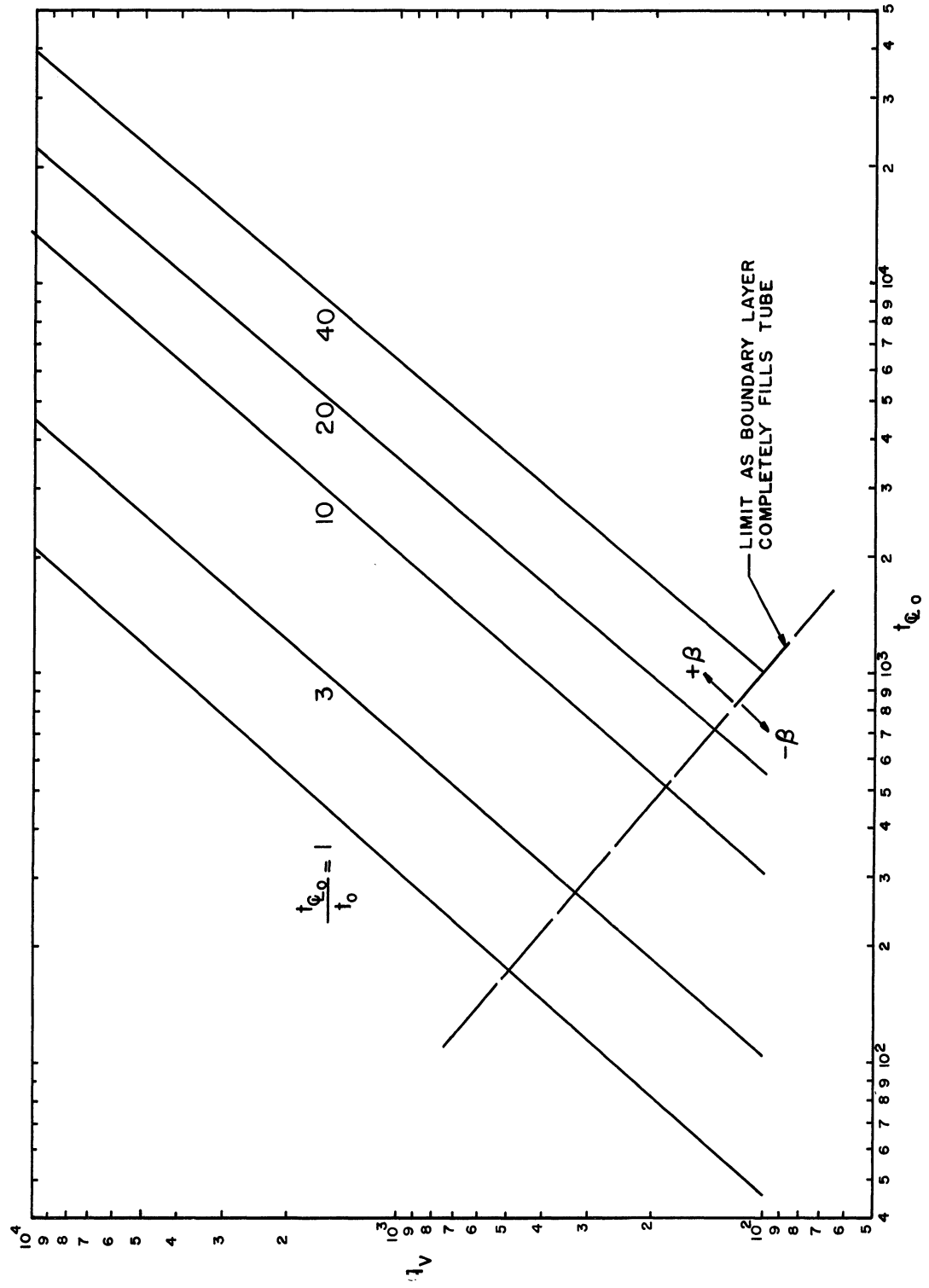

Figure 3. Non-Dimensional Heat Source Strength Vs. Non-Dimensional Maximum Temperature Differential.

These slopes are very close to those found in Reference 2 and the change in the intercept is only slightly greater. Therefore, it appears that the values of k and n of Reference 2 can be used to a good approximation for the wall temperature and heat source distributions not covered in this report.

The boundary layer thickness, Figure 4, increases more rapidly at the lower heat source strengths. Whereas for $q_v = 1 \times 10^4$ the boundary layer fills 55 percent of the tube for the constant wall temperature case, it fills 88 percent of the tube at $q_v = 1 \times 10^3$, and for $q_v = 1 \times 10^2$ the boundary layer has crossed the tube centerline and, if such could be tolerated, fills 142 percent of the tube. This point can easily be seen by the rapidly decreasing slope of a plot of q_v vs. the maximum boundary layer (Figure 5). From this curve, as mentioned previously, it can be seen that the boundary layer just fills the tube at a heat source strength of about 5×10^2.

Figures 6a, b, and c show that the increase in boundary layer thickness due to linear variation of the wall temperature is also larger at the lower q_v's. In all cases, the lowering of q_v causes a progression up the tube of the point of maximum boundary layer thickness. At $q_v = 1 \times 10^6$, $(1 - \beta)_{max}$ occurred at $x/l = 0.85$ (Reference 2), while at a $q_v = 1 \times 10^2$, $(1 - \beta)_{max}$ had progressed to $x/l = 0.40$, again considering the constant wall temperature case as typical.

The axial temperature distributions are shown in Figure 7 as the ratio t_{ℓ} / t_{ℓ_o}, i.e. the non-dimensional temperature difference from the centerline at any axial position to the wall at the bottom as related to the maximum value, from the centerline at the top of the cylinder to the wall at the bottom.

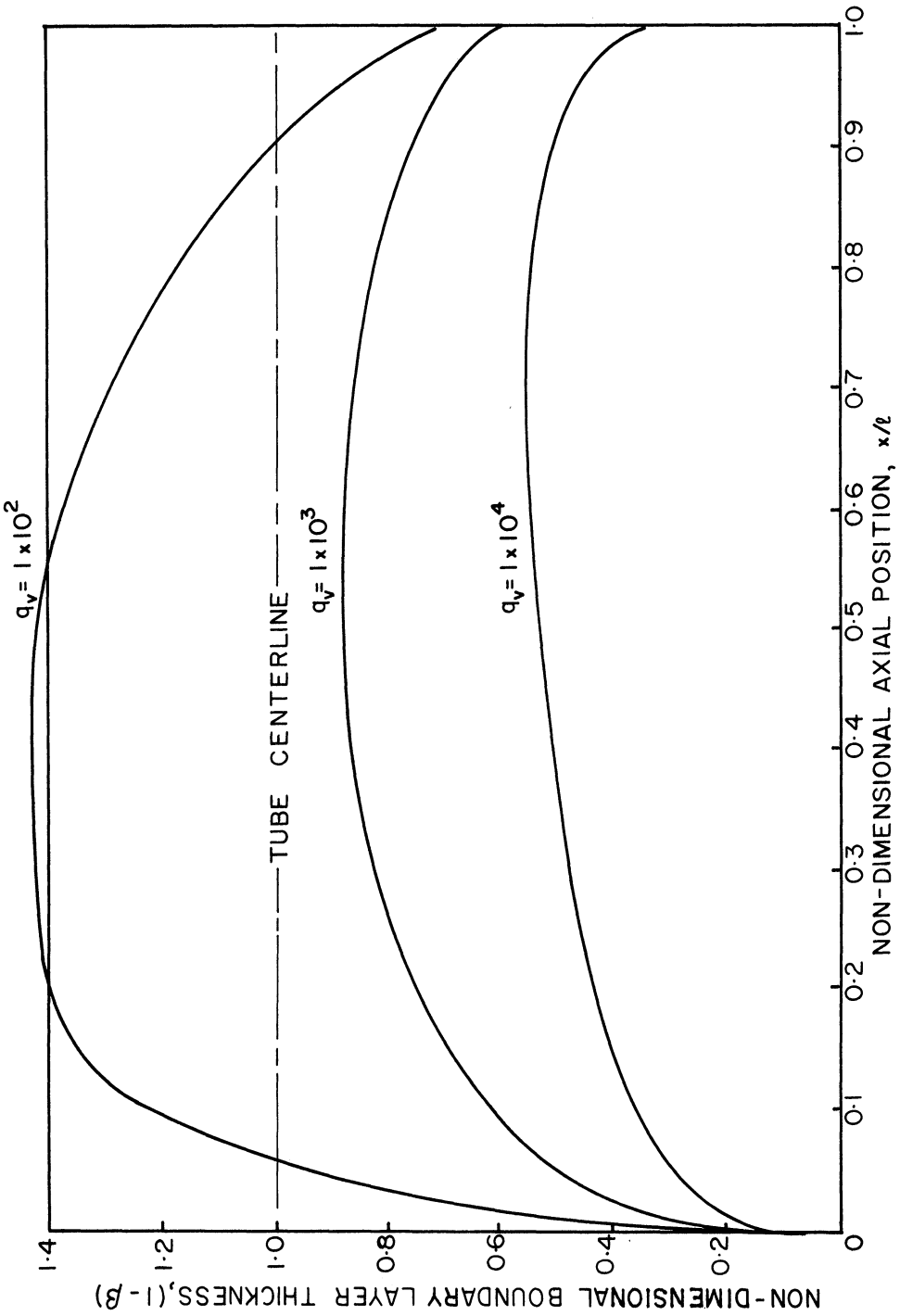

Figure 4. Non-Dimensional Boundary Layer Thickness Vs. Axial Position, Constant Wall Temperature.

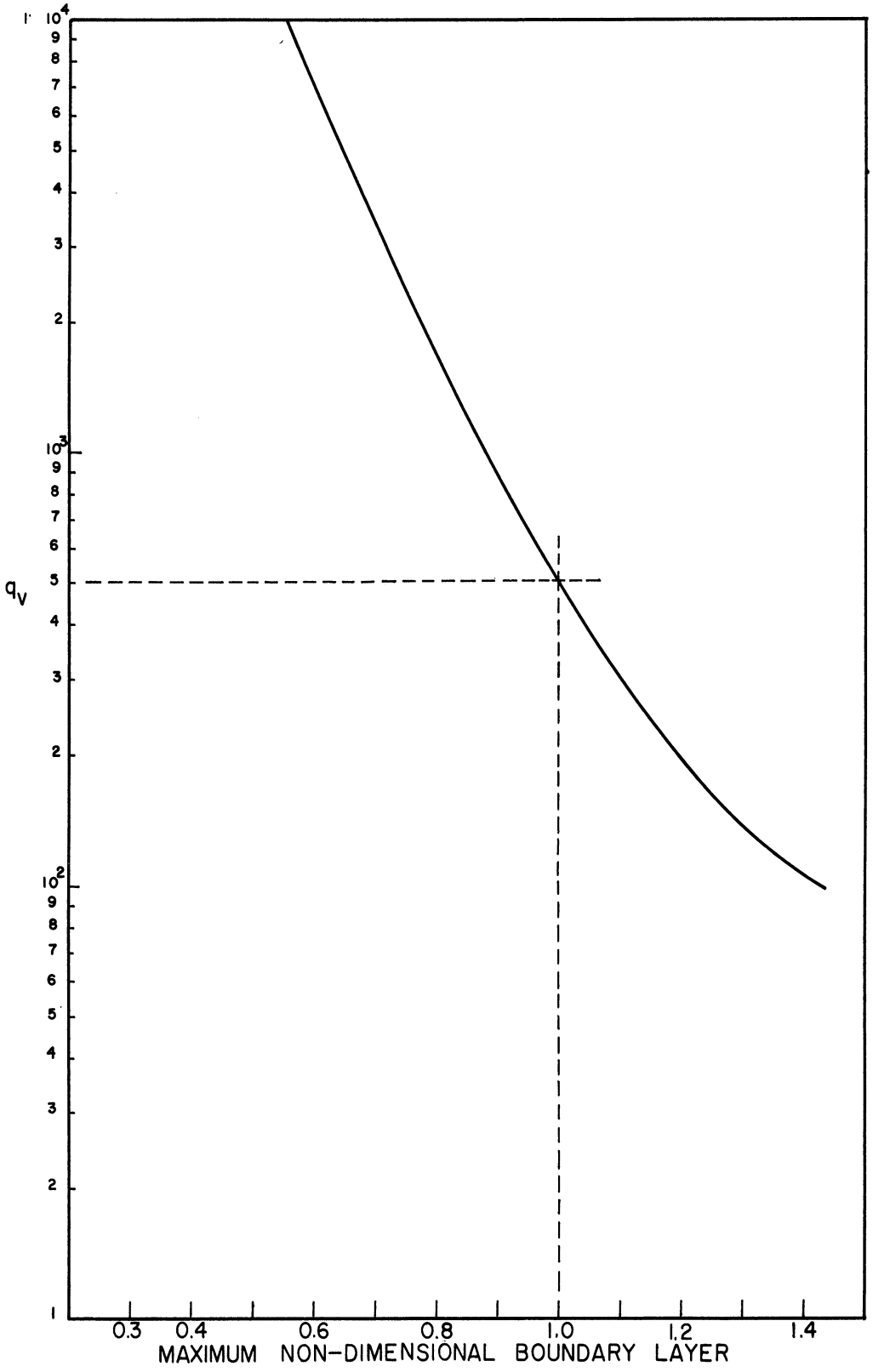

Figure 5. Non-Dimensional Heat Source Strength Vs. Maximum Non-Dimensional Boundary Layer Thickness, Constant Wall Temperature.

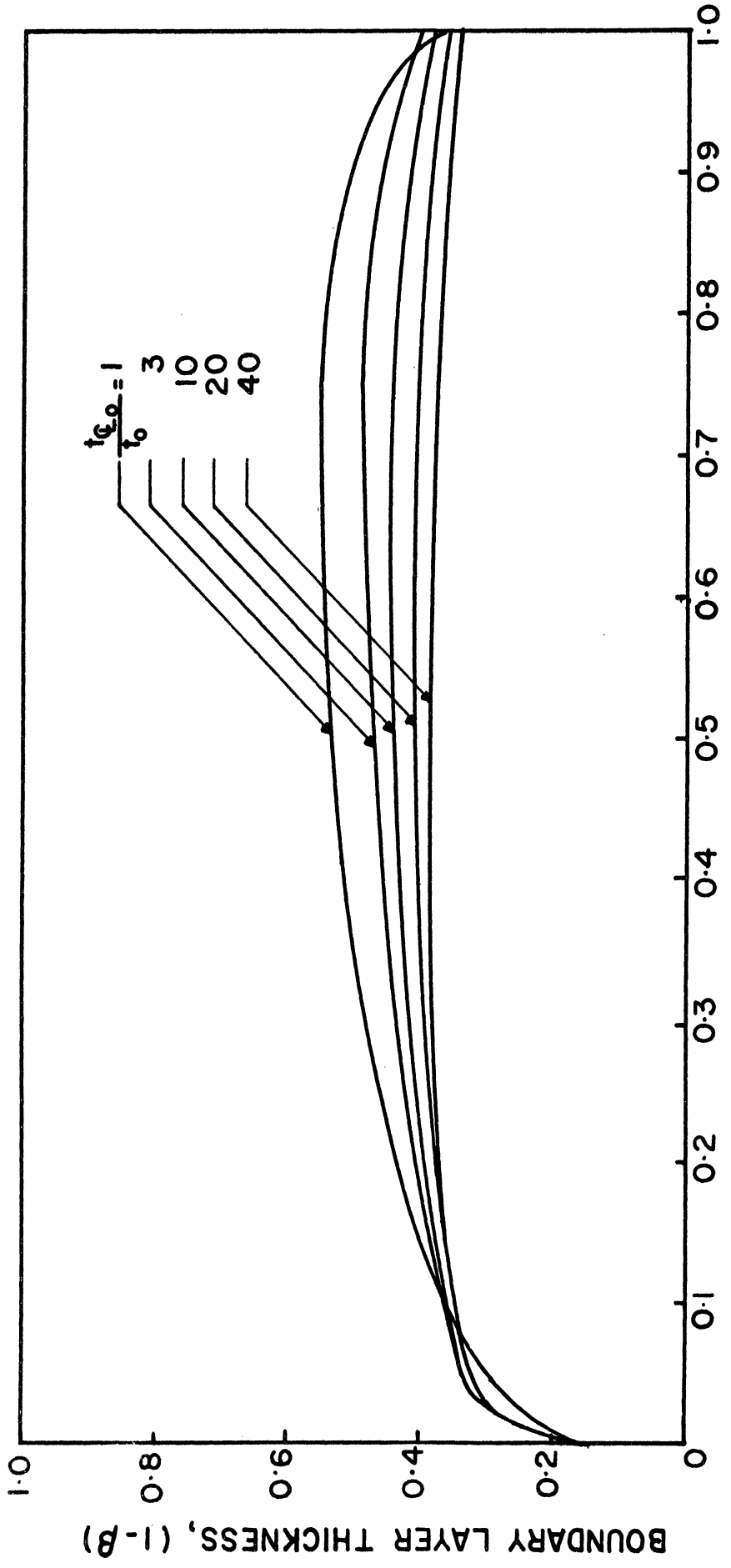

Figure 6a. Non-Dimensional Boundary Layer Thickness Vs. Axial Position, Linear Variable Wall Temperature, $q_v = 1 \times 10^4$.

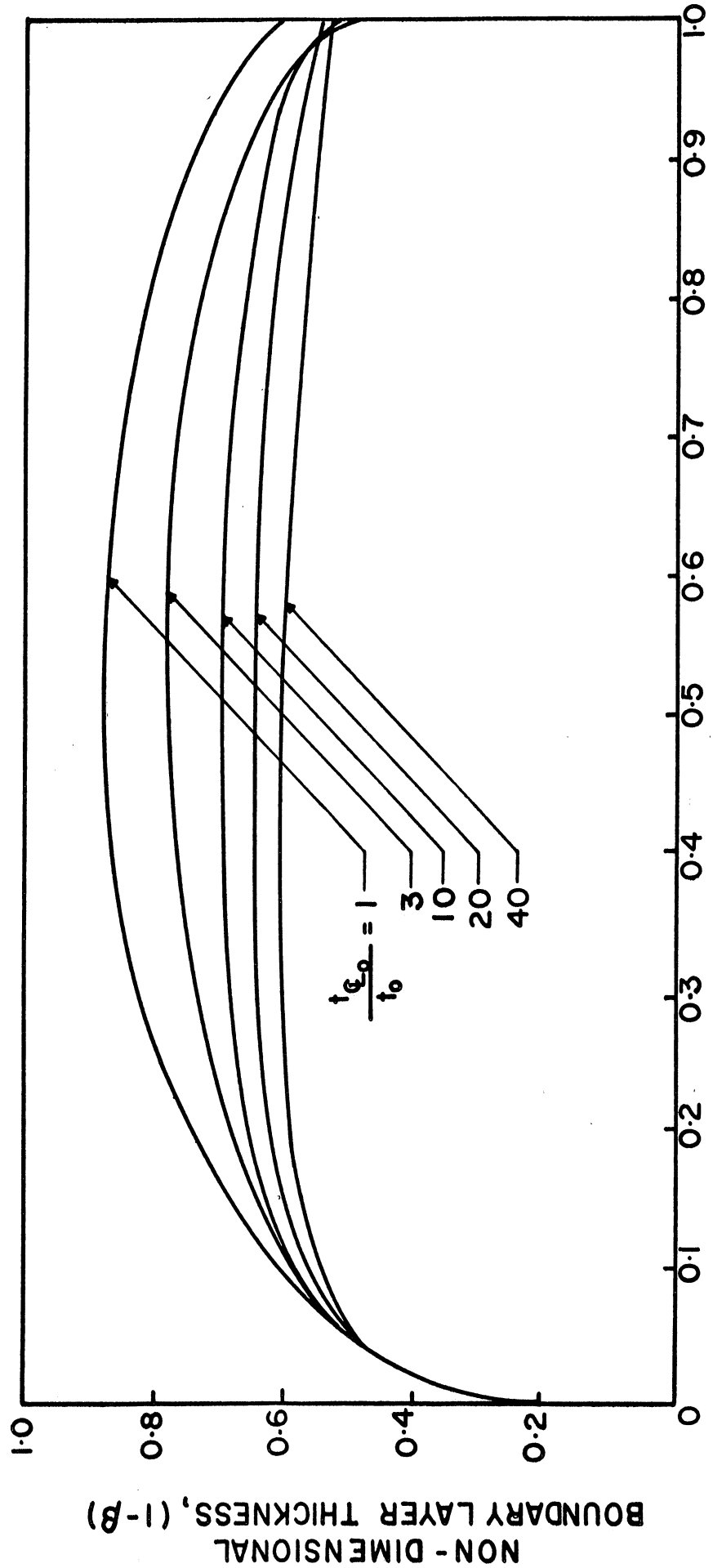

Figure 6b. Non-Dimensional Boundary Layer Thickness Vs. Axial Position, Linear Variable Wall Temperature, $q_v = 1 \times 10^3$.

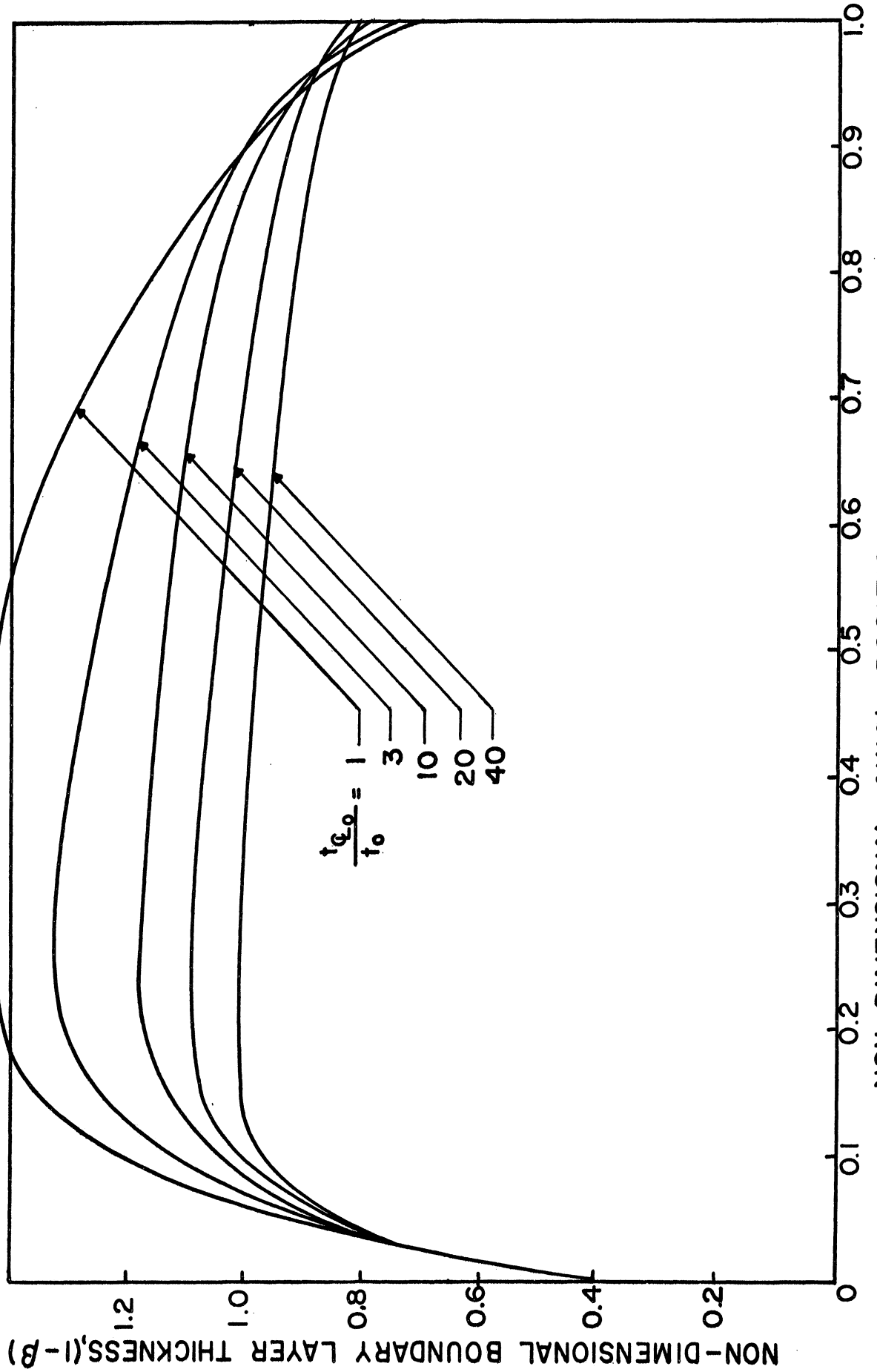

Figure 6c. Non-Dimensional Boundary Layer Thickness Vs. Axial Position, Linear Variable Wall Temperature, $q_v = 1 \times 10^3$.

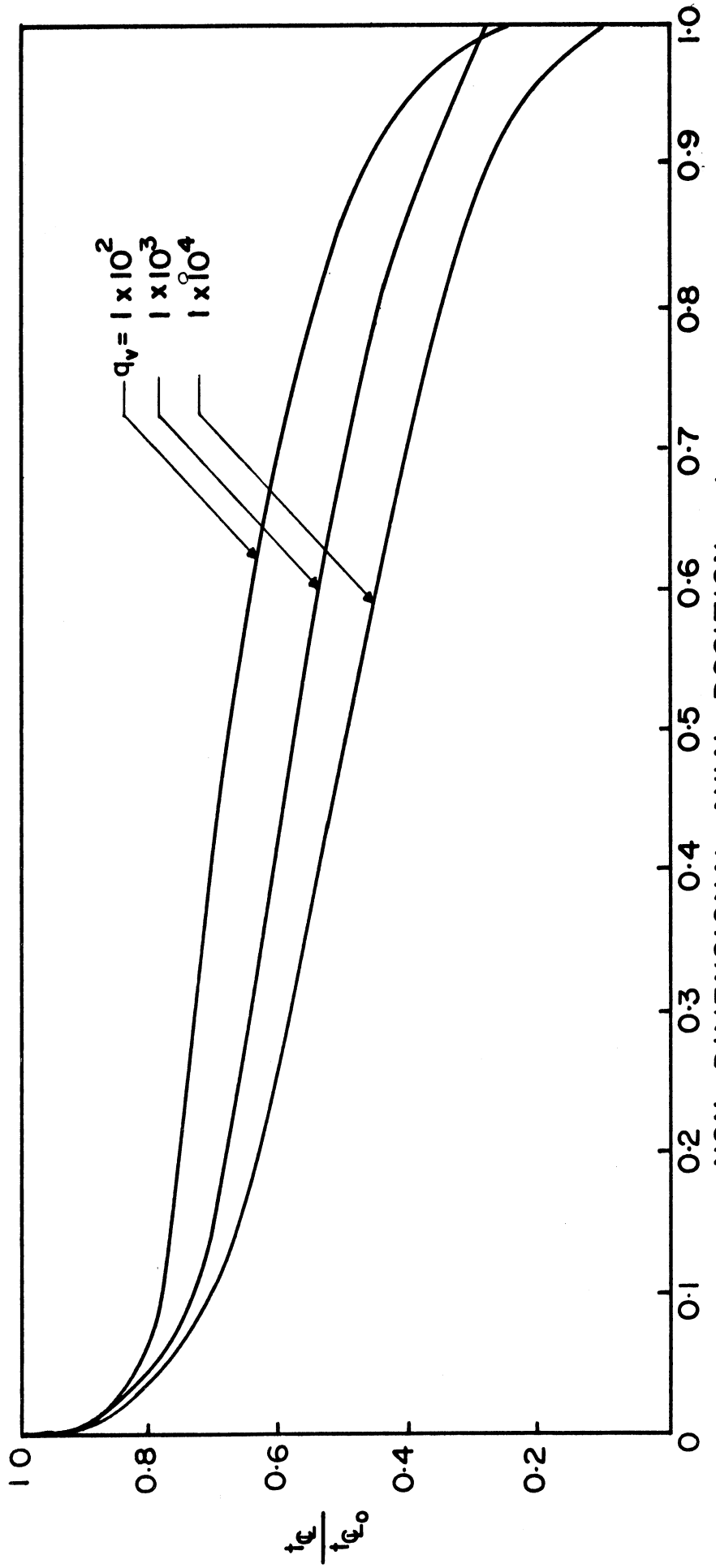

Figure 7a. Non-Dimensional Centerline Temperature Distribution Vs. Axial Position, Constant Wall Temperature.

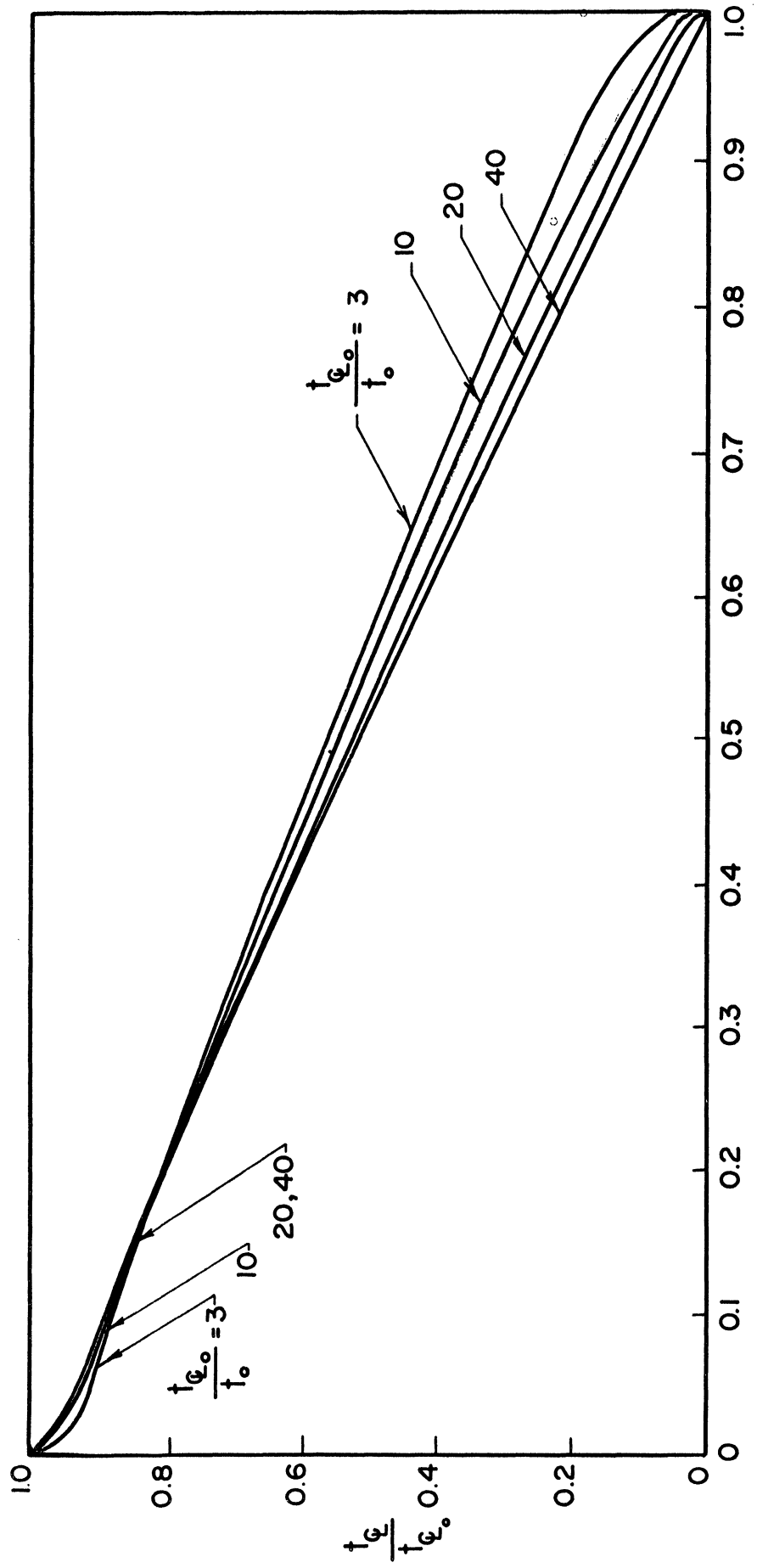

Figure 7b. Linear Variable Wall Temperature, $q_v = 1 \times 10^4$.

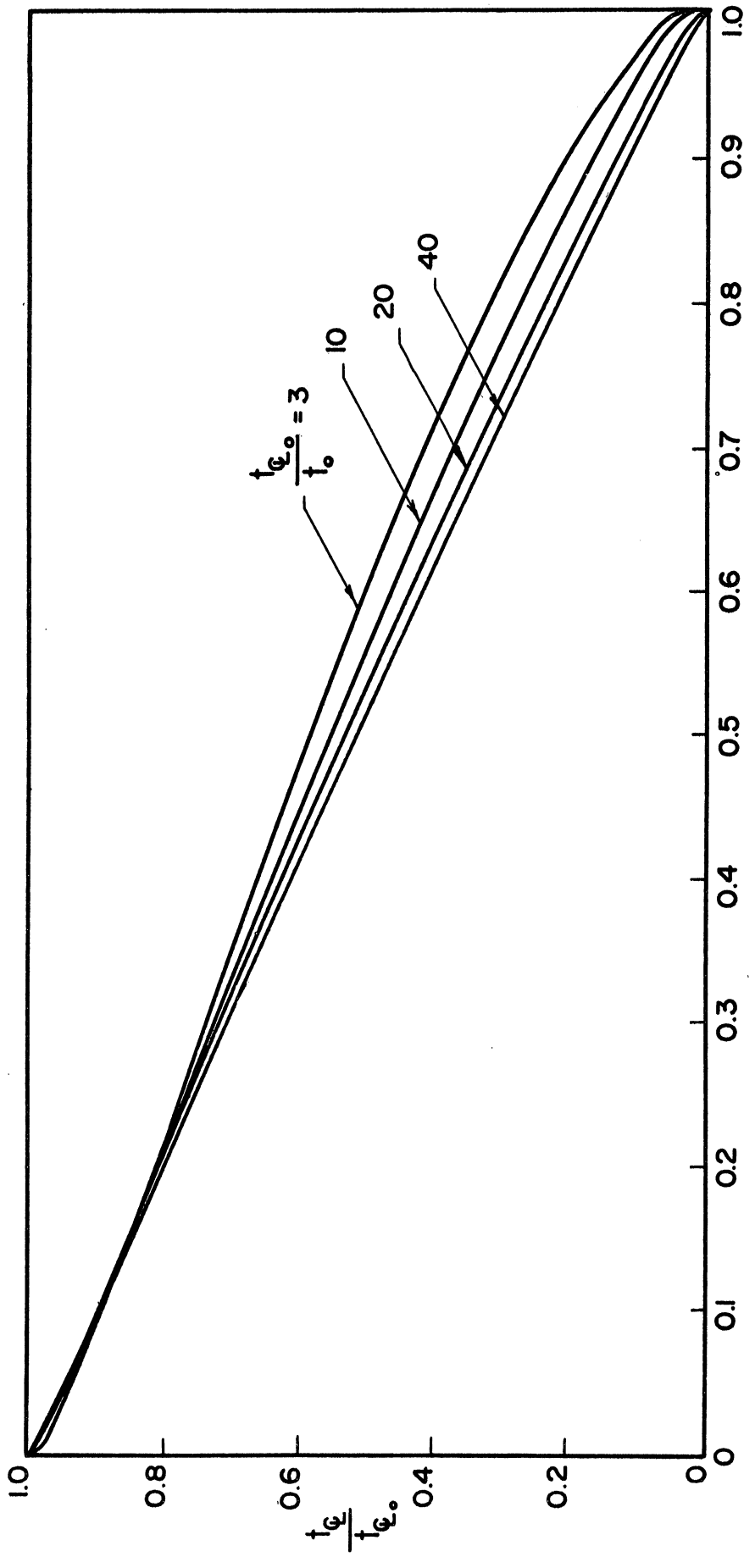

Figure 7c. Linear Variable Wall Temperature, $q_V = 1 \times 10^3$.

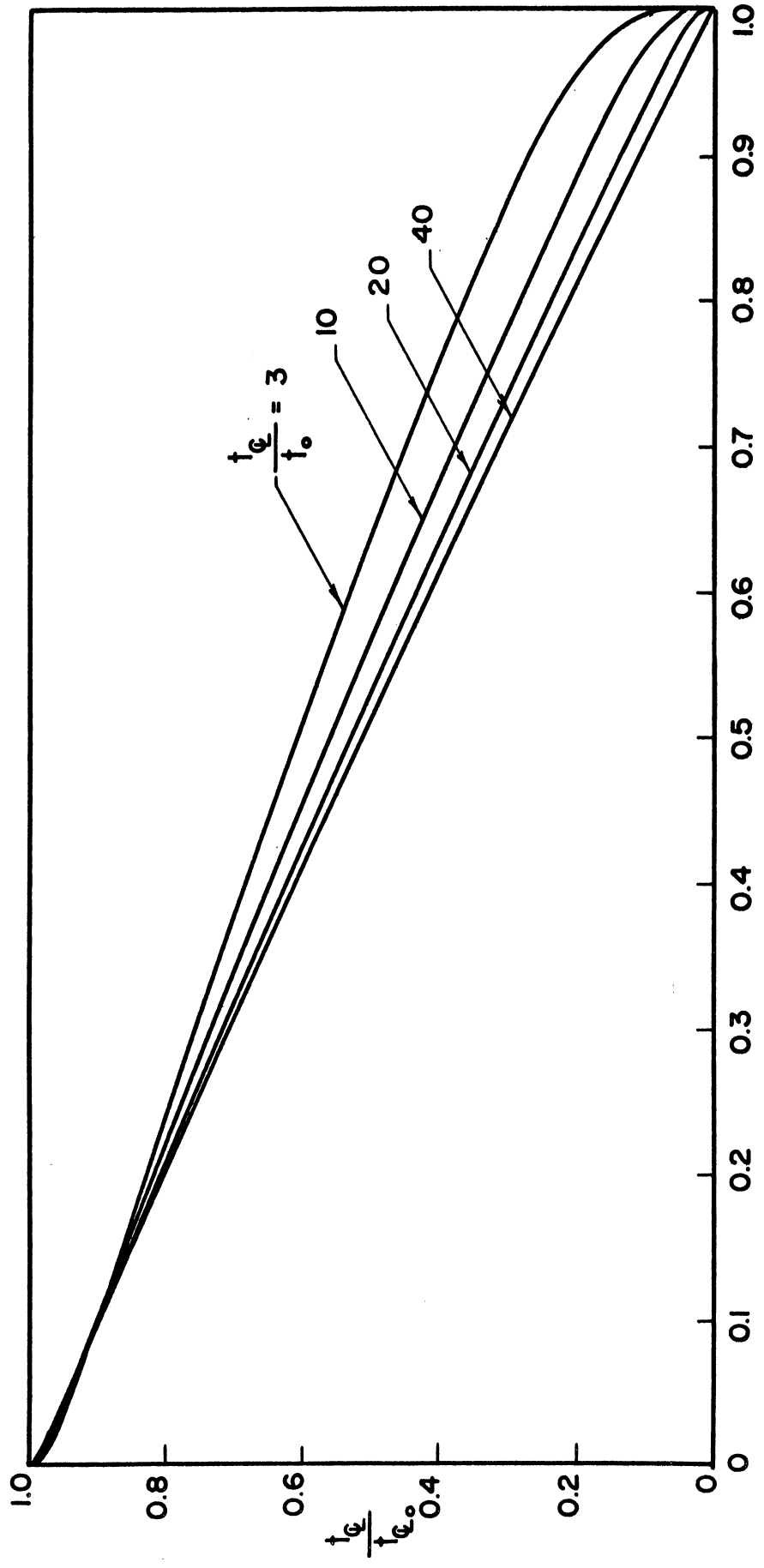

Figure 7d. Linear Variable Wall Temperature, $q_v = 1 \times 10^2$.

At the higher values of q_V (Figure 29a, Reference 2) there was a small increase in t_{ℓ}/t_{ℓ_o} with decreasing q_V, approximately 27% over the q_V range 2 x 10^9 to 1 x 10^5, or roughly four decades, at x/l = 0.7. At the lower q_V range, 1 x 10^4 to 1 x 10^2, or only two decades, the similar increase in t_{ℓ}/t_{ℓ_o} is of the order of 50% or approximately an increase of a factor of four.

The variable wall temperature runs produced the same effect, i.e. a pronounced increase in the spread of t_{ℓ}/t_{ℓ_o} for wall temperature variations from 3 to 40 at the lower q_V's compared to the high q_V range. The spread of t_{ℓ}/t_{ℓ_o} for t_{ℓ_o}/t_o from 3 to 40 at a q_V = 1 x 10^4 is about 26% while at q_V = 1 x 10^2 the spread has increased to about 45%. All the trends indicated in Reference 2 at the high q_V range are corrborated by this supplementary data in the low q_V range.

The radial temperature distributions, t/t_{ℓ_o}, show little difference for the q_V range presented in this report (Figure 8) from the higher q_V range. In all cases, the curves for t_{ℓ_o}/t_o of 10, 20, and 40 are close to horizontal. The curve for t_{ℓ_o}/t_o = 3 shows best the tendency for a rapid decrease in temperature at the top and bottom, with the intermediate section nearly constant.

For the constant wall temperature case $t = t_{\ell}$, since t_w, in the general relation $t + t_w = t_{\ell}$, equals zero. Therefore, the plots of t_{ℓ}/t_{ℓ_o}, previously discussed, are identical to these for the special case of constant wall temperature.

The wall heat flux is presented vs. axial position in the tube in terms of the function normalized to the value at the axial midpoint

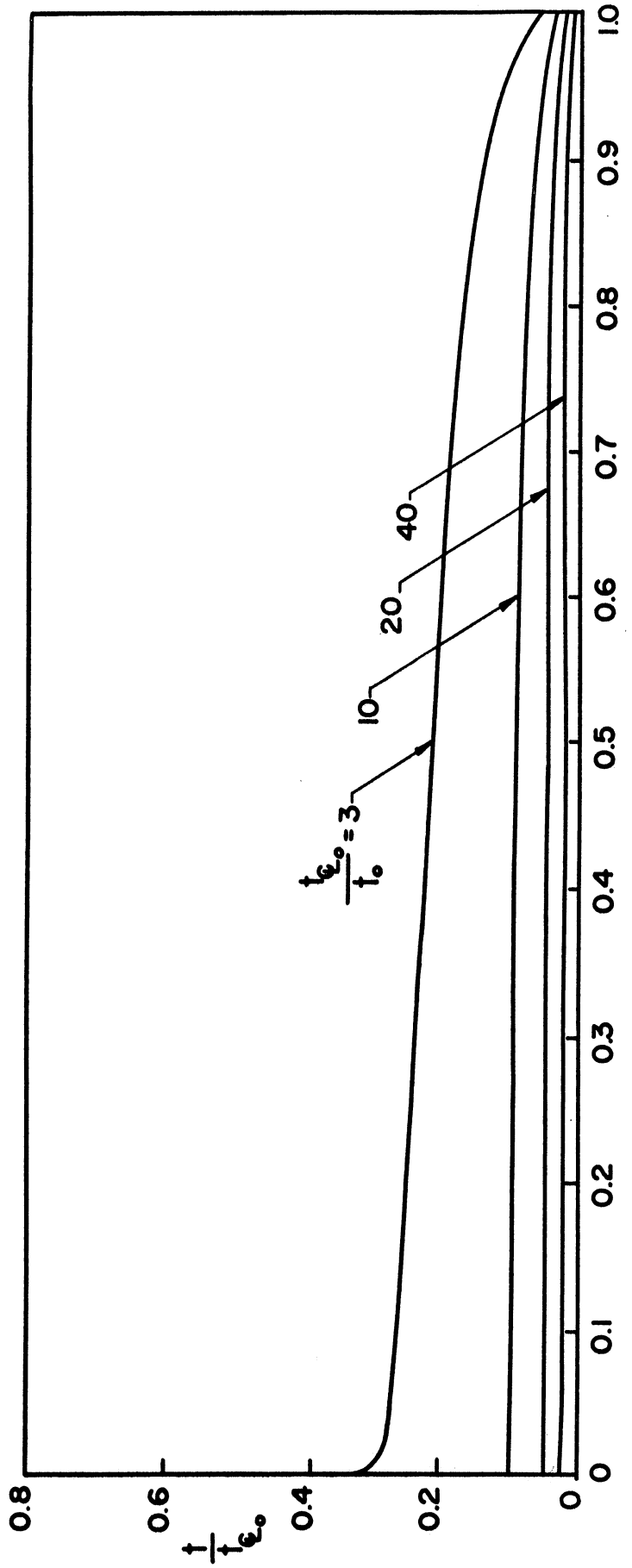

Figure 8a. Non-Dimensional Radial Temperature Differential Vs. Axial Position, Linear Variable Wall Temperature, $q_v = 1 \times 10^4$.

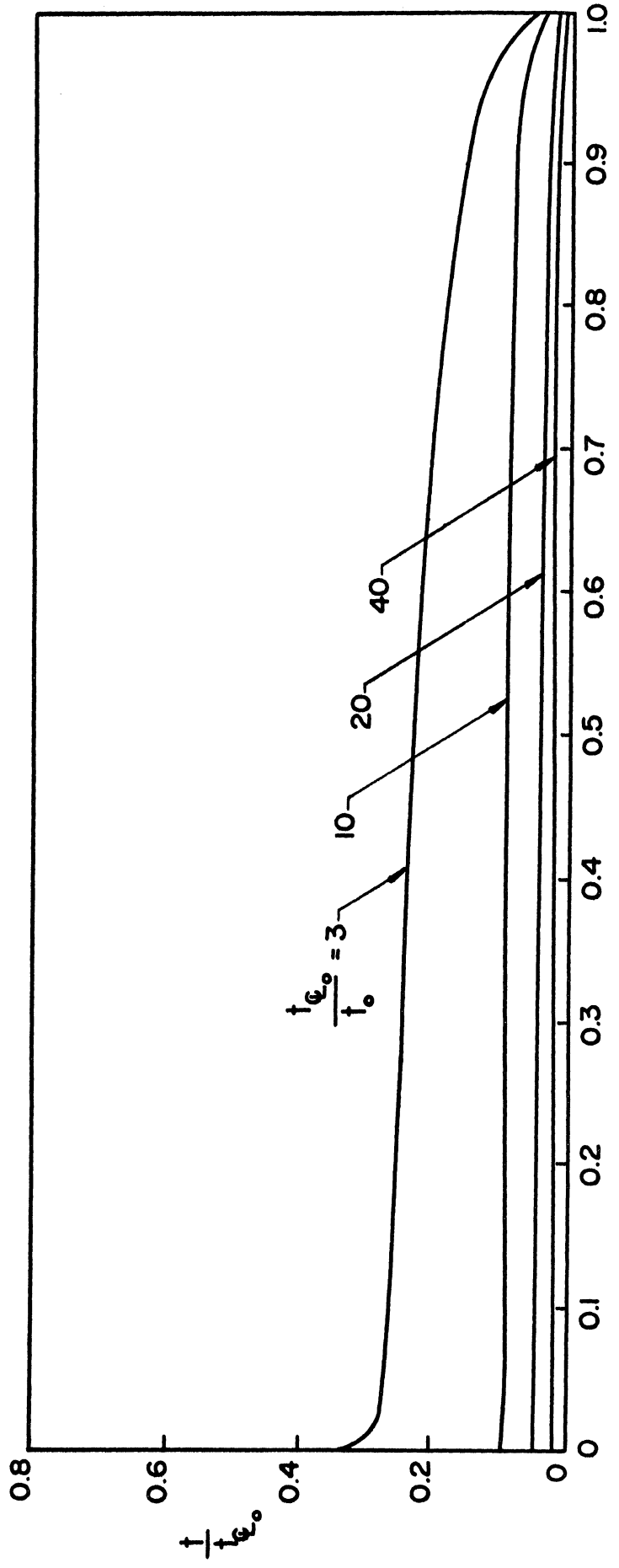

Figure 8b. Non-Dimensional Radial Temperature Differential Vs. Axial Position, Linear Variable Wall Temperature, $q_v = 1 \times 10^3$.

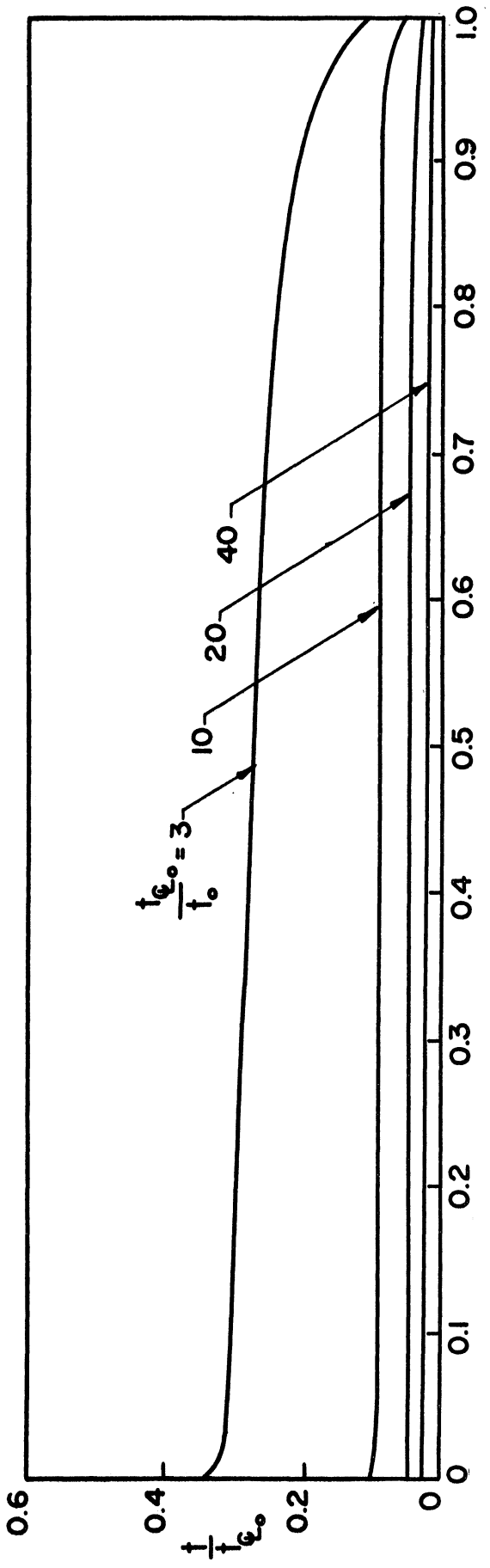

Figure 8c. Non-Dimensional Radial Temperature Differential Vs. Axial Position, Linear Variable Wall Temperature, $q_V = 1 \times 10^2$.

of the tube, x/l = 0.50. Figure 9a shows the results for a constant wall temperature. Again, as with the other parameters discussed, the rapidity with which the normalized wall conduction approaches the limiting condition of low q_v is apparent. The limiting condition, in this case, is a horizontal line at 1.0, which according to the mathematics of the problem would represent a boundary layer completely filling the tube radially and axially.

The effects of low q_v and consequently a large boundary layer on the wall conduction can be derived from Equation (11). The wall conduction term $\frac{t_N + t_{N-1}}{2-\beta_N-\beta_{N-1}}$ reduces to a constant, t, for constant wall temperatures as approaches zero and the boundary layer, $1-\beta$, approaches 1.0. The constant, t, is very small because the heat source is small. The non-dimensional function, $G(\beta)$, increases rapidly as β decreases, from 10^{-8} at $\beta = 0.99$ to 0.1 at $\beta = 0$. This causes the $\frac{4 q_v \Delta x}{t_{\ell N-1}^2 (G_N + G_{N-1})}$ term in Equation (12) to become very small and thus the square root to approach 1.0. Thus, $t_{\ell N} = t_{\ell N-1}$, or since the wall temperature is constant, $t_N = t_{N-1}$. When normalized to the axial middle of the test section or the point where the boundary layer initially approaches the centerline, the length of tube over which the wall conduction is constant will appear as a line at 1.0. The axial portion of the tube over which this occurs increases with decreasing q_v. The limit axially would occur when the wall conduction became constant over the entire length of the tube.

It should be noted that the plots shown are not for the limiting case of fully developed boundary layer but rather show the results of negative boundary layer thickness for the low q_v and hence are not physically significant. Nevertheless, the results approach those expected for the fully developed boundary layer.

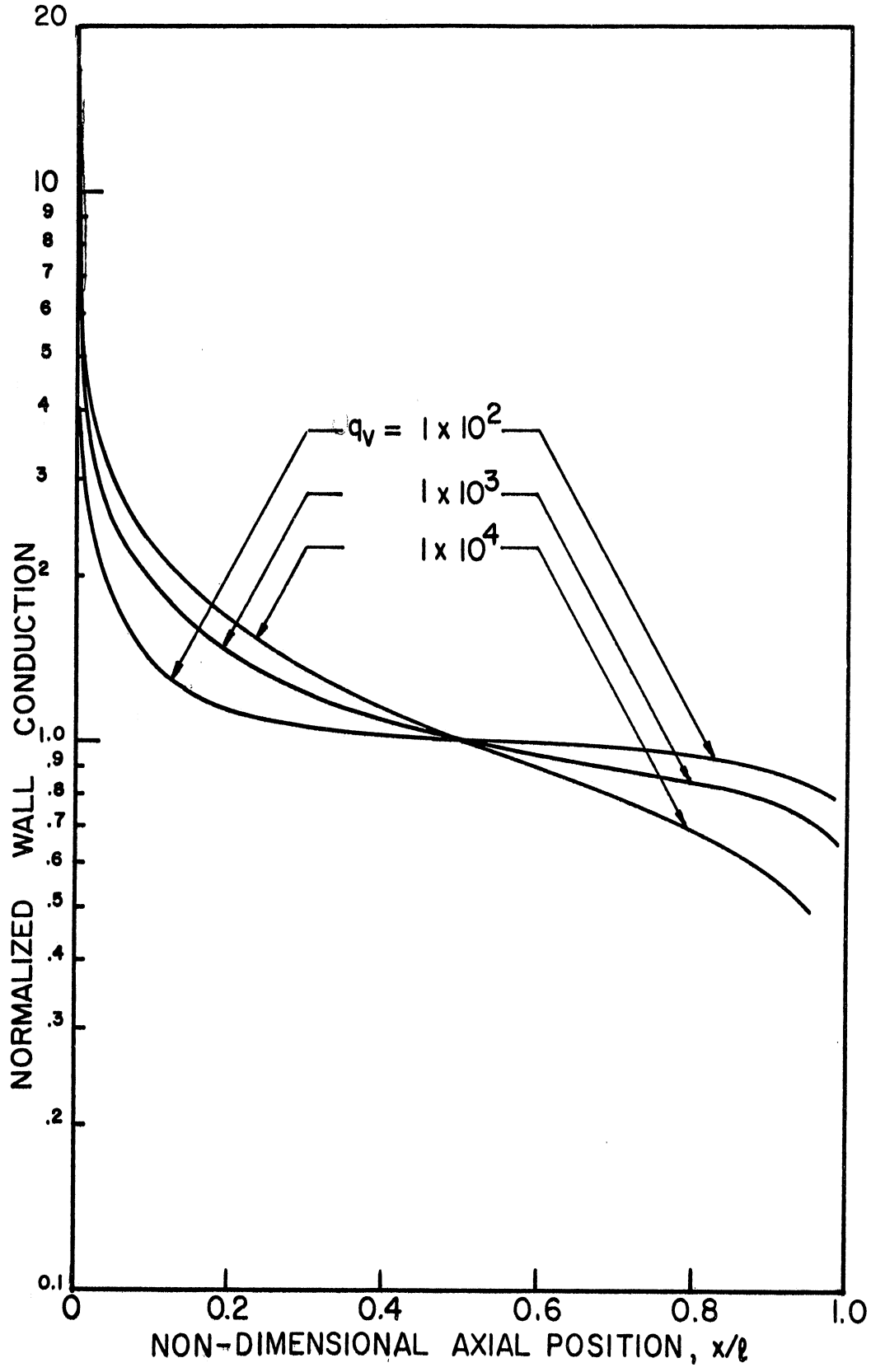

Figure 9a. Normalized Wall Conduction Vs. Axial Position, Constant Wall Temperature.

The variable wall temperature case presented in Figures 9b, c, and d is somewhat more complicated. Now, especially for large t_{ℓ_o}/t_o ratios, the progression toward a constant wall conduction term is even more rapid. The significance of a large ratio of t_{ℓ_o}/t_o is that the wall temperature differential is increasingly larger than the radial temperature differential and, hence, becomes the dominent factor. Although the wall temperature does not enter Equation (11) directly, it does enter the second equation, (12). Therefore, it indirectly effects the wall conduction term through the radial temperature, t. This is apparent by a comparison of Figures 9b and 9d.

The fluid velocities attained in both the core and the boundary layer are shown in Figure 10a. The boundary layer velocity calculated is the maximum value based on the assumed profile (Figure 2), and occurs relatively near the tube wall. In Reference 2 it was noted that the core velocity was always less than the boundary layer velocity and that the ratio of boundary layer/core velocity decreased with decreasing q_v. This same trend continues into the lower q_v range, however, at a q_v of 1×10^4, with a constant wall temperature, where the boundary layer and core each occupy roughly 50% of the tube radially, the velocities are approximately equal (Figure 10b). As the q_v becomes even lower, and the core occupies a smaller part of the tube, the core velocity becomes greater than the boundary layer velocity. The ratio of boundary layer velocity to core velocity while approximately 1 at $q_v = 1 \times 10^4$ is 0.39 at $q_v = 1 \times 10^3$ and 0.12 at $q_v = 1 \times 10^2$ for the constant wall temperature case.

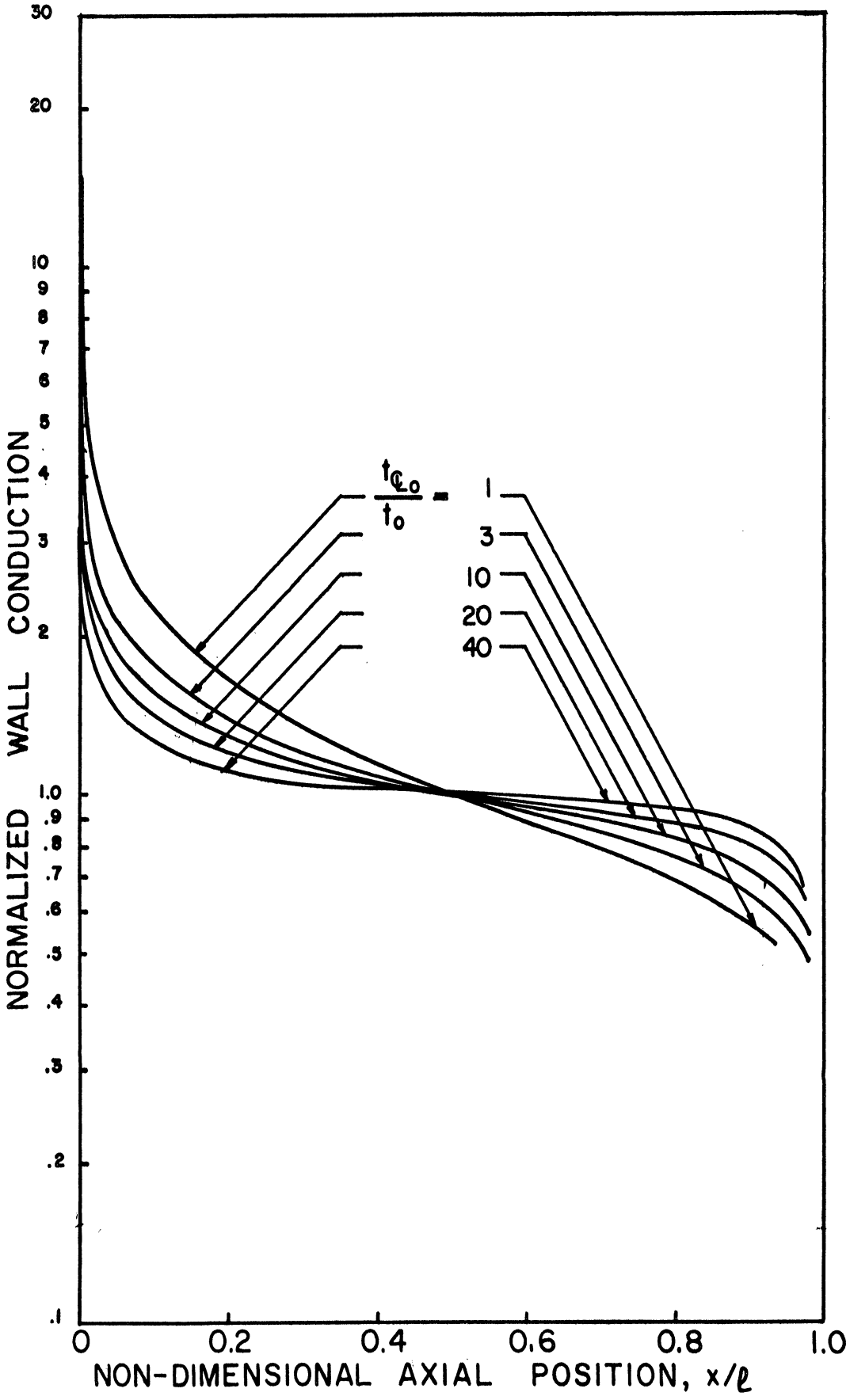

Figure 9b. Linear Variable Wall Temperature, $q_v = 1 \times 10^4$.

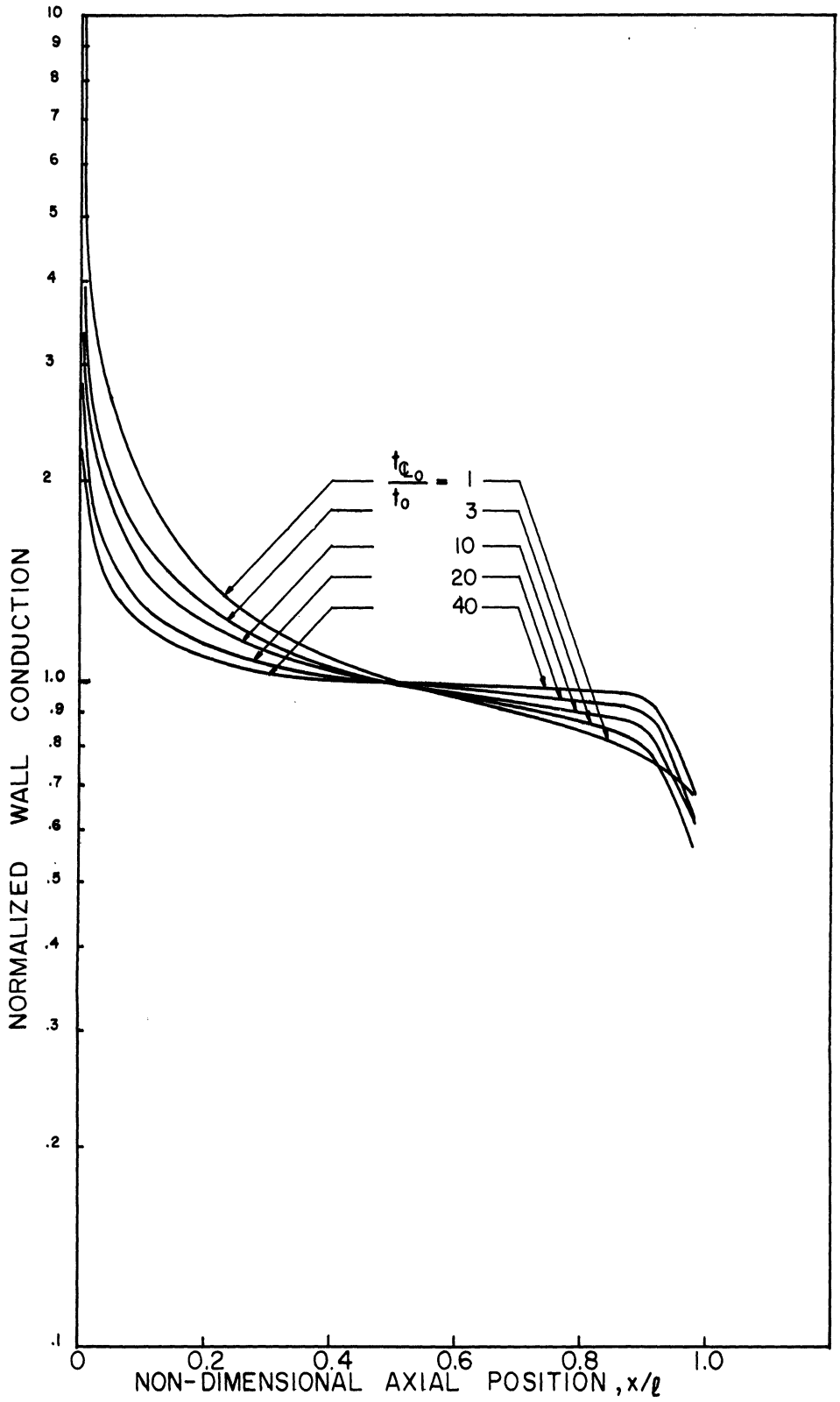

Figure 9c. Linear Variable Wall Temperature, $q_v = 1 \times 10^3$.

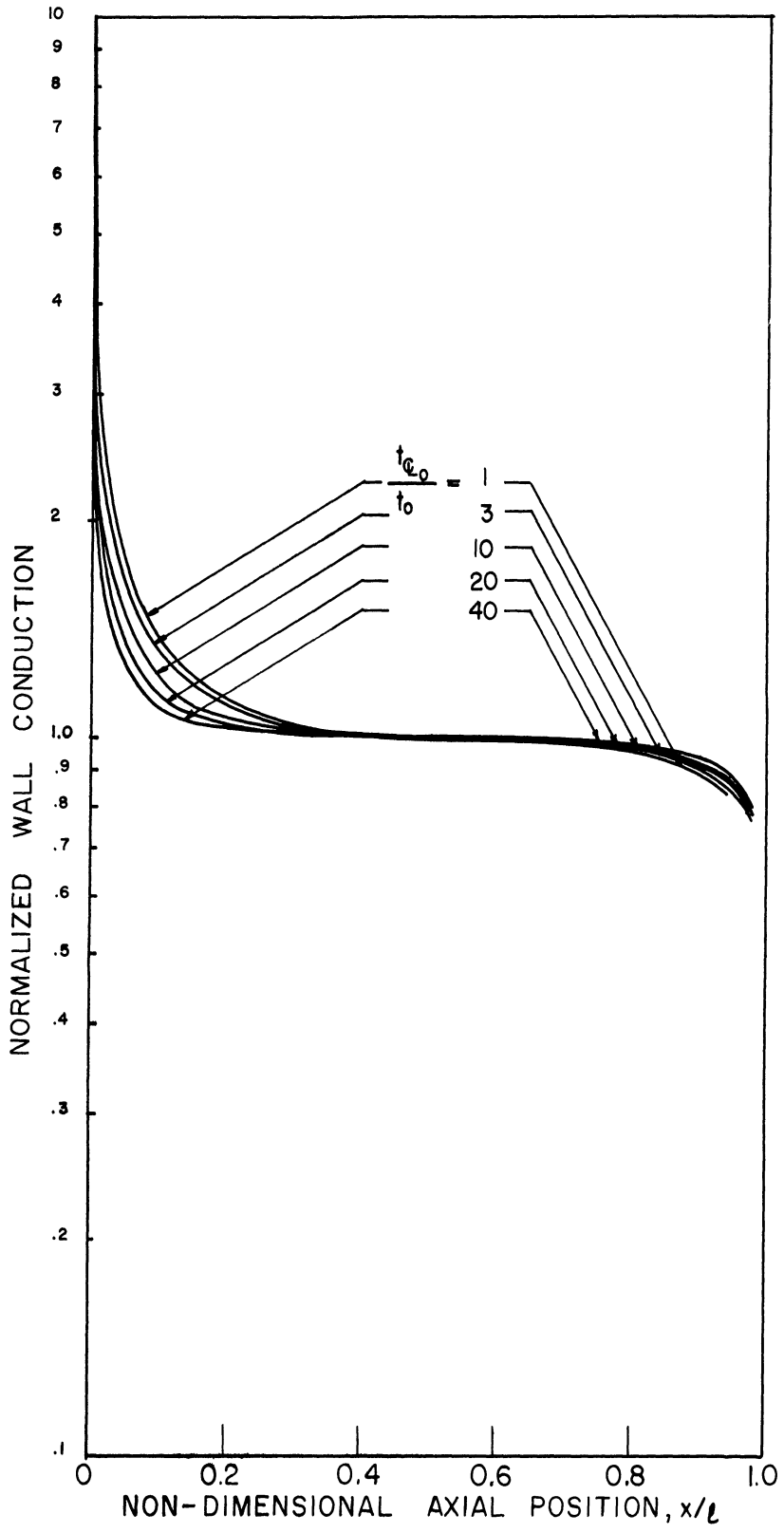

Figure 9d. Linear Variable Wall Temperature, $q_v = 1 \times 10^2$.

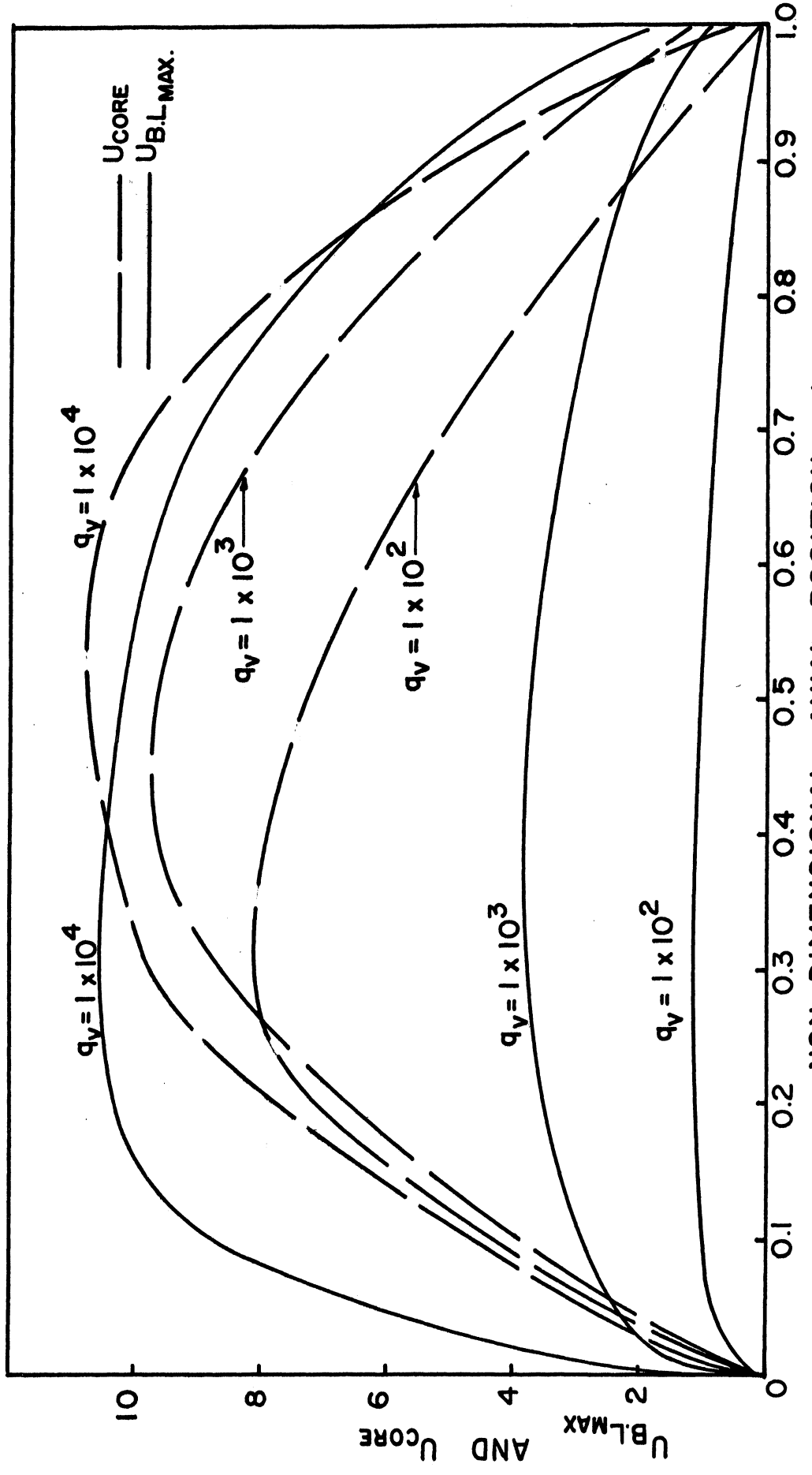

Figure 10a. Non-Dimensional Boundary Layer and Core Velocity Vs. Axial Position, Constant Wall Temperature.

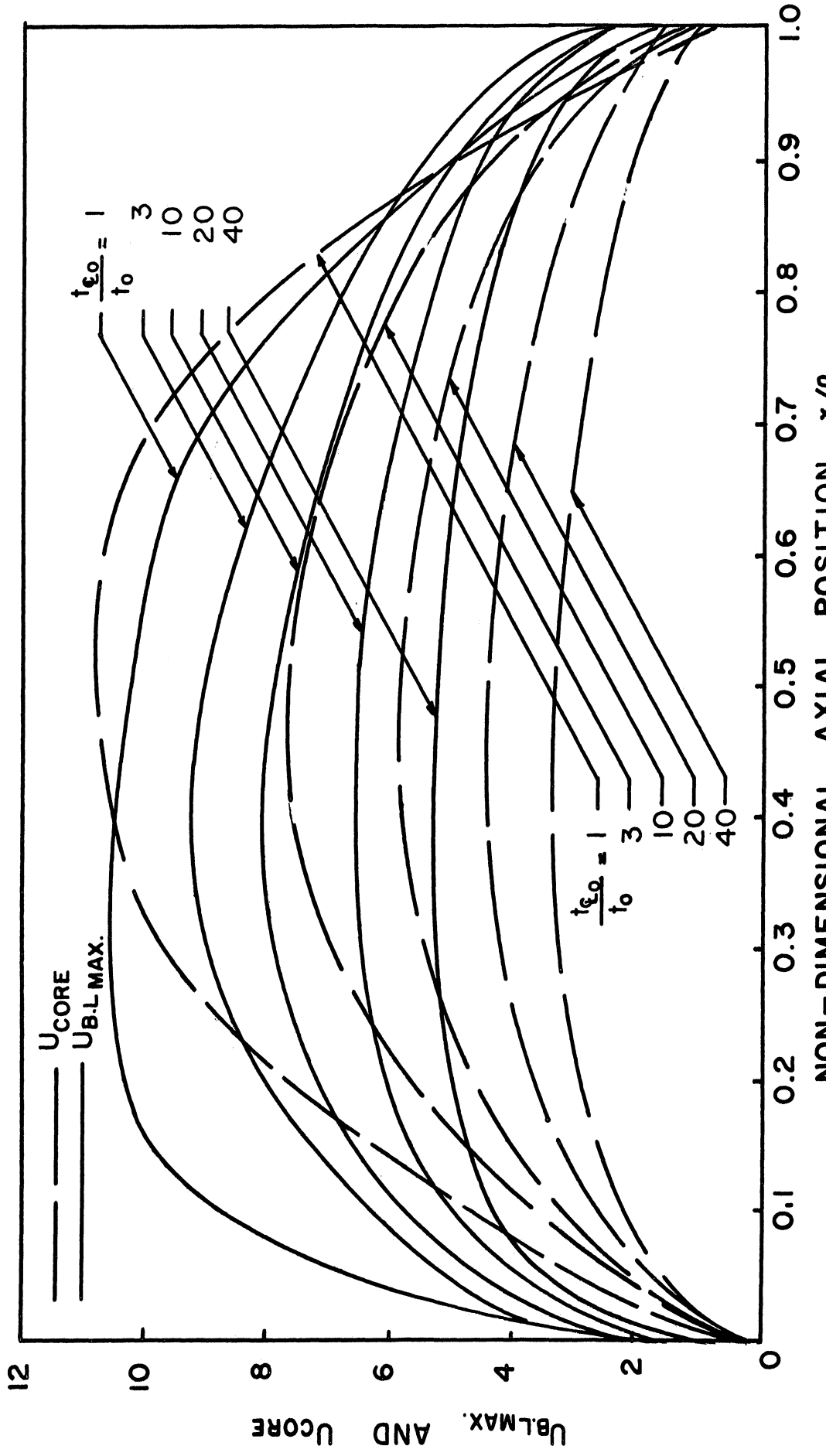

Figure 10b. Linear Variable Wall Temperature $q_v = 1 \times 10^2$.

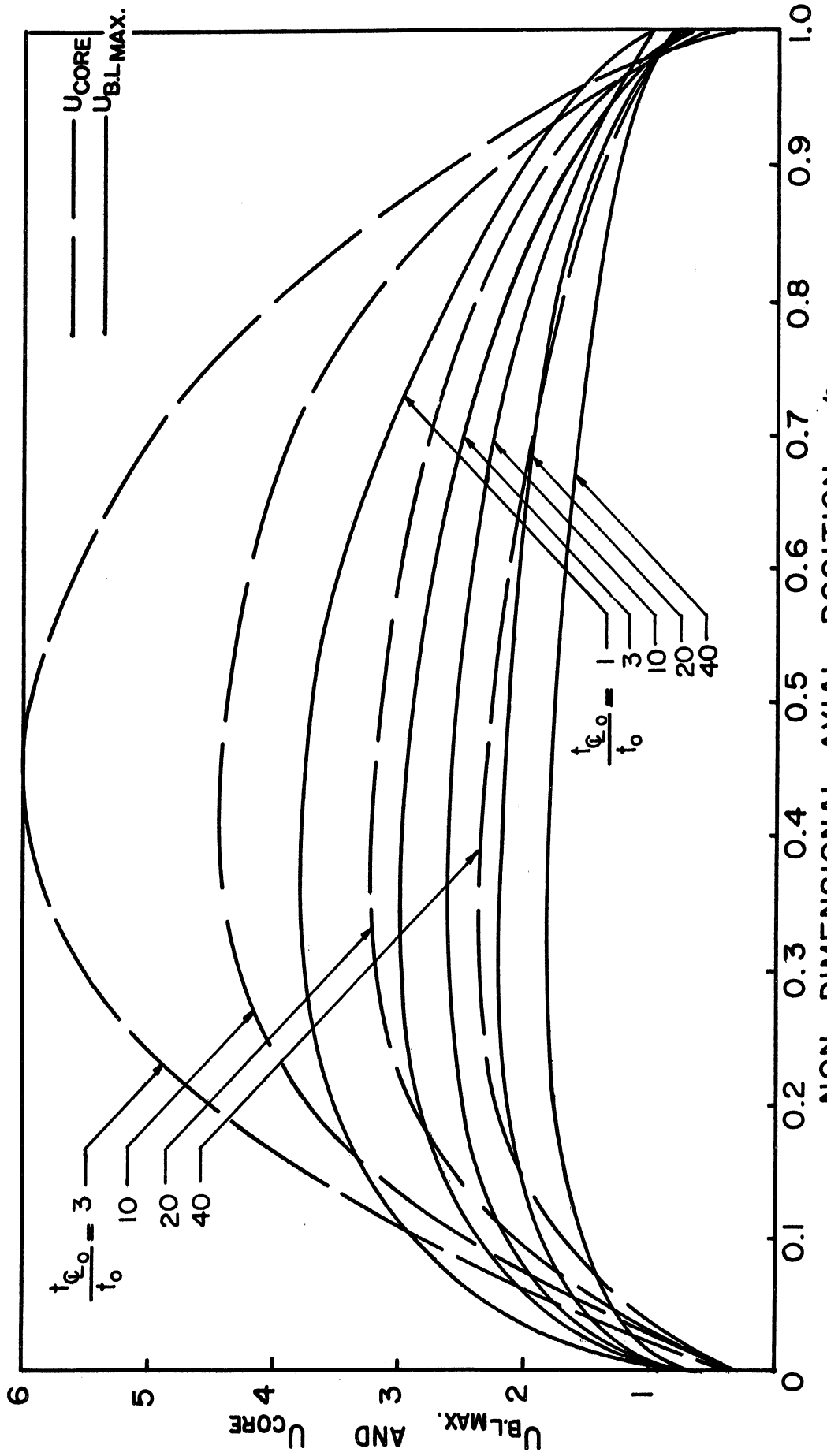

Figure 10c. Linear Variable Wall Temperature, qv = 1 x 10^3.

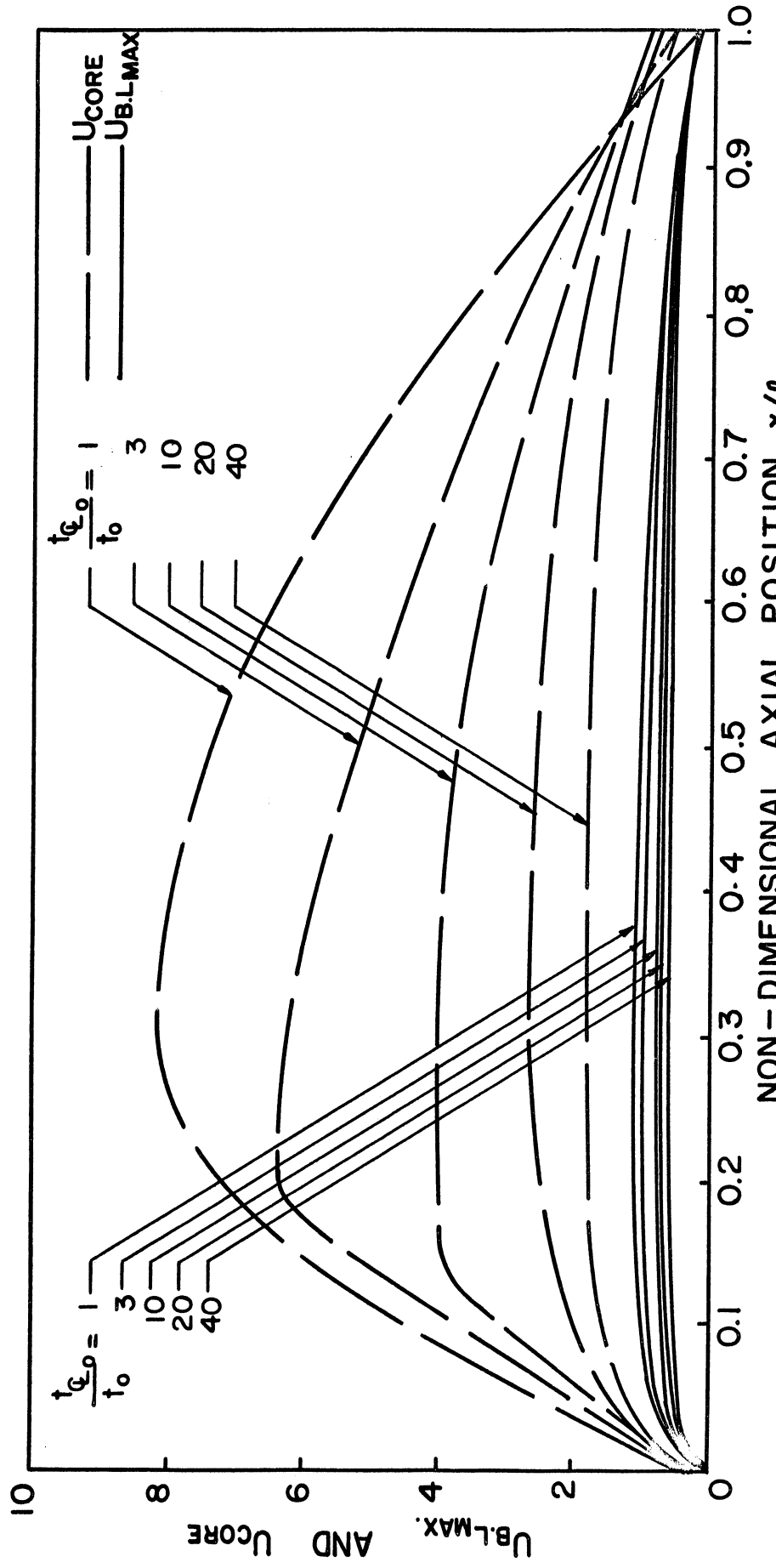

Figure 10d. Linear Variable Wall Temperature qv = 1 x 10^2.

The variation of $u_{BL_{max}}$ and u_{core} with q_v and β noted here can be derived directly from the basic velocity profile assumption. This is shown in the Appendix. The velocity profile shown in Figure 2 and expressed by Equation (4) yields the following relationship between $u_{BL_{max}}$ and u_{core} across the tube.

Boundary Layer	$u_{BL_{max}}/u_{core}$
0.25	2.798
0.50	1.062
0.75	0.518
1.00	0.280

Thus, when the boundary layer fills the tube, the velocity in the core is 3.6 times the maximum boundary layer velocity.

The general trend is the same for the variable wall temperature case. However, for any one heat source strength the boundary layer and core velocities are more nearly equal at the larger temperature ratios, t_{ℓ_o}/t_o. This is simply a function of the fact that the boundary layer thickness increases less rapidly as t_{ℓ_o}/t_o increases.

The absolute value of the non-dimensional velocities is much larger at heat source strengths of 1×10^6 and higher (Reference 2) than in the range considered here. Also, the ratio of boundary layer to core velocity has a much greater rate of change at the higher q_v condition than at the very low q_v. This is inherently a function of the basic velocity assumptions, manifested through the $G(\beta)$, $\gamma = G(\beta)\, t$, term in the velocity profile.

CONCLUSIONS

The general trends and empirical relations found in Reference 2 for a range of high heat source strength can be accurately extended to the lower q_v range for the cases considered. It may now be assumed that this will hold true for wall temperature distributions and heat source distributions other than those considered in this report.

The rate at which the boundary layer increases is more rapid once it has occupied approximately half of the tube. As an effect of this then, the rates of change of temperature, velocity, and wall conduction are all increased. At a non-dimensional heat source strength of about 5×10^2 the boundary layer completely fills the tube. At this point, the equations and assumptions on which this analysis is based no longer apply and a new system must be constructed.

APPENDIX

Derivation of Energy Relation for Radial Disc for Variable Wall Temperature Condition

From Reference 1, an energy balance for a disc (Figure 1) is

$$\rho c_v \left[\frac{\partial}{\partial X}\int_0^a UT2\pi R\,dR\right]\Delta x = k\left(\frac{\partial T}{\partial R}\right)_{R=a}\Delta x\, 2\pi a + Q_v \pi a^2 \Delta x \qquad (A1)$$

$$\frac{\partial}{\partial X}\int_0^a 2UTR\,dR = 2\frac{k}{\rho c_v}a\left(\frac{\partial T}{\partial R}\right)_{R=a} + a^2\frac{Q_v}{\rho c_v} \qquad (A2)$$

Substitute

$$X = xl$$

$$R = ra$$

$$T = T_{WALL\,MIN} - \frac{\nu\kappa l}{\alpha g a^4}(t_r + t_w)$$

$$U = \frac{\kappa l}{a^2}u$$

Then

$$\frac{1}{\rho}\frac{\partial}{\partial x}\int_0^1 2\frac{\kappa l}{a^2}u\left[T_{WALL\,MIN} - \frac{\nu\kappa l}{\alpha g a^4}(t_r + t_w)\right] r a\, d(ra) =$$

$$2\frac{\kappa q}{a}\frac{\partial}{\partial r}\left[T_{WALL\,MIN} - \frac{\nu\kappa l}{\alpha g a^4}(t_r + t_w)_{r=1}\right] + a^2\frac{Q_v}{\rho c_v} \qquad (A3)$$

But

$$\frac{\partial}{\partial x}\left(T_{WALL\,MIN}\right) = 0$$

$$\frac{\partial}{\partial r}\left(T_{WALL\,MIN}\right) = 0$$

Therefore

$$-\frac{\partial}{\partial x}\int_0^1 (t_r + t_w)\, u\, r\, dr = \frac{\partial}{\partial r}(t_r + t_w)_{r=1} - \frac{1}{2}\,\frac{a^2 \alpha q a^4}{\kappa^2 \ell \rho_V}\,\frac{Q_V}{\rho c_v} \qquad (A4)$$

t_w does not vary with respect to r, but does vary with respect to x.

$$\frac{\partial}{\partial x}\int_0^1 u(t_r + t_w)\, r\, dr = \frac{\partial}{\partial r}(t_r)_{r=1} - \frac{1}{2}\rho_V \qquad (A5)$$

$$\left(\frac{\partial t_r}{\partial r}\right)_{r=1} = -t_A\left\{2\left(\frac{r-\beta}{1-\beta}\right)\left(\frac{1}{1-\beta}\right)\right\}_{r=1} \qquad (A6)$$

$$= -\frac{2t_A}{1-\beta} \qquad (A7)$$

$$\frac{\partial}{\partial x}\int_0^1 u t_r\, r\, dr + \frac{\partial}{\partial x}\int_0^1 u t_w\, r\, dr = \frac{\partial}{\partial x}\int_0^\beta u t_r\, r\, dr +$$

$$\frac{\partial}{\partial x}\int_\beta^1 u t_r\, r\, dr + \frac{\partial}{\partial x}\int_0^\beta u t_w\, r\, dr + \frac{\partial}{\partial x}\int_\beta^1 u t_w\, r\, dr \qquad (A8)$$

Substituting the assumed velocity and temperature profiles

$$u = \begin{cases} -\gamma & 0 < \beta < r \\ -\gamma \left[1 - \left(\frac{r-\beta}{1-\beta} \right)^2 1 + \delta(r-1) \right] & \beta < r < 1 \end{cases}$$

$$t = \begin{cases} t_A & 0 < \beta < r \\ t_A \left[1 - \left(\frac{r-\beta}{1-\beta} \right)^2 \right] & \beta < r < 1 \end{cases}$$

(A9)

$$\underbrace{\frac{\partial}{\partial x}\int_0^{\beta} -\gamma t_A r\, dr + \frac{\partial}{\partial x}\int_{\beta}^{1} -\gamma \left[1 - \left(\frac{r-\beta}{1-\beta} \right)^2 \{1 + \delta(r-1)\} \right] t_A \left[1 - \left(\frac{r-\beta}{1-\beta} \right)^2 \right] r\, dr}_{\text{I}}$$

$$\underbrace{\frac{\partial}{\partial x}\int_0^{\beta} -\gamma t_w r\, dr + \frac{\partial}{\partial x}\int_{\beta}^{1} -\gamma \left[1 - \left(\frac{r-\beta}{1-\beta} \right)^2 \{1 + \delta(r-1)\} \right] t_w r\, dr}_{\text{II}}$$

For constant wall temperature

$t_w = 0$

$t_A = t$ (does not vary with x)

But for variable wall temperature

$t_w = f(x)$

$t_A = f(x)$

f(x) is some function of x/l

As derived by Lighthill, Part I of Equation (A9) becomes

$$-2\frac{d}{dx}\left[t_A^{\,2}\,F(\beta)\right] \tag{A10}$$

where

$$F(\beta) = \frac{(1-\beta)^3(3+\beta)(45+132\beta+181\beta^2+62\beta^3)}{30240(3+4\beta+3\beta^2)}$$

Part II of Equation (A9) becomes

$$\frac{\partial}{\partial x}\;-\gamma t_w\int_0^{\beta} r\,dr\;+\int_{\beta}^{1}\left[1-\left(\frac{r-\beta}{1-\beta}\right)^2\left\{1+\delta(r-1)\right\}\right]r\,dr \tag{A11}$$

which equals

$$\frac{\partial}{\partial x}\left(-\gamma t_w\right)H(\beta,\delta) \tag{A12}$$

where

$$H(\beta,\delta) = \frac{1}{2} - \frac{1}{(1-\beta)^2}\left(\frac{1}{4}-\frac{2\beta}{3}+\frac{\beta^2}{2}-\frac{\beta^4}{12}\right) + \frac{\delta}{(1-\beta)^2}\left(\frac{1}{20}-\frac{\beta}{6}+\frac{\beta^2}{6}-\frac{\beta^4}{12}+\frac{\beta^5}{30}\right) \tag{A13}$$

From References 1 and 2

$$\gamma = t_A\,G(\beta)$$

where

$$G(\beta) = \frac{(3+\beta)(3+2\beta)(1-\beta)^3}{36(3+4\beta+3\beta^2)}$$

Thus, Equation (A12) which is Part II of Equation (A9) equals

$$- \frac{\partial}{\partial x} \left\{ G(\beta)\, H(\beta,\delta)\, t_A\, t_w \right\} \tag{A14}$$

And Equation (A5) becomes

$$\frac{d}{dx} \left[2 t_A^2 F(\beta) + G(\beta)\, H(\beta,\delta)\, t_A\, t_w \right] = - \frac{2 t_A}{(1-\beta)} + \frac{q_v}{2} \tag{A15}$$

Substituting $\delta = - \dfrac{5(3+2\beta+\beta^2)}{(1-\beta)^2 (3+2\beta)}$ (Reference 1)

in Equation (A15) and solving, the second term on the left side drops out

So that (A5) is

$$\frac{d}{dx} \left[t_A^{\,2} F(\beta) \right] = \frac{t_A}{(1-\beta)} - \frac{q_v}{4} \tag{A16}$$

where t_A can be replaced by $t(x)$ indicating variation with x.

Derivation of Maximum Boundary Layer Velocity

The maximum velocity in the boundary layer will occur where $\dfrac{\partial u}{\partial r} = 0$ (Figure 2). Thus, differentiating the velocity equation for the boundary layer

$$\frac{\partial u}{\partial r} = \frac{2\gamma}{(1-\beta)^2} (r-\beta) + \frac{\delta\gamma}{(1-\beta)^2} (3r^2 - 4r\beta - 2r + 2\beta + \beta^2) \tag{A17}$$

Setting this equal to zero, the radial distance at which the velocity is maximum is

$$r_{u_{BL\,MAX}} = \frac{\beta}{3} - \frac{0.667}{\delta} + 0.667 \tag{A18}$$

Since the core velocity = γ , the ratio of $u_{BL_{max}}/\gamma$ is the ratio of the maximum boundary layer velocity to the core velocity. This is found for any β by substituting $r_{uBL_{max}}$ and β into the velocity equation for the boundary layer.

$$\frac{u_{BL\,MAX}}{\gamma} = -\left[1-\left(\frac{r-\beta}{1-\beta}\right)^2\{1+\delta(r-1)\}\right] \qquad \text{(A19)}$$

TABLE I - SUMMARY OF RESULTS

UNIFORM q_w ; CONSTANT WALL TEMPERATURE

Variable	Run / x/ℓ	1	2	Run / x/ℓ	3
	0	1.000	1.000	0	1.000
	0.001	0.8828	0.8080	0.001	0.6803
	0.01	0.8031	0.6736	0.003	0.5944
	0.05	0.6998	0.4952	0.01	0.4411
	0.20	0.5656	0.2589	0.03	0.2177
β	0.40	0.4871	0.1381	0.07	-0.0748
	0.60	0.4527	0.1250	0.13	-0.3218
	0.80	0.4590	0.1863	0.25	-0.4074
	0.90	0.4937	0.2491	0.40	-0.4193
	0.96	0.5509	0.3112	0.65	-0.3294
	0.999	——	0.3837	0.90	-0.0059
	1.000	1.000	1.000	0.999	0.3389
				1.000	1.000
	0	2.1246×10^{3}	3.150×10^{2}		
	0.001	2.022×10^{3}	2.996×10^{2}	0	46.05
	0.01	1.853×10^{3}	2.756×10^{2}	0.001	43.87
	0.05	1.639×10^{3}	2.475×10^{2}	0.003	42.42
t	0.20	1.356×10^{3}	2.145×10^{2}	0.01	40.37
	0.40	1.135×10^{3}	1.901×10^{2}	0.03	38.28
	0.60	0.948×10^{3}	1.687×10^{2}	0.07	36.79
	0.80	0.734×10^{3}	1.416×10^{2}	0.13	35.70
	0.90	0.579×10^{3}	1.209×10^{2}	0.25	34.12
	0.96	0.416×10^{3}	1.016×10^{2}	0.40	32.22
	0.999	——	0.806×10^{2}	0.65	28.50
	1.000	0	0	0.90	21.56
				0.999	9.56
	0	35.40×10^{3}	3.502×10^{2}	1.000	0
	0.001	12.34×10^{3}	11.09×10^{2}		
	0.01	7.025×10^{3}	6.293×10^{2}	0	28.13×10
	0.05	4.077×10^{3}	3.708×10^{2}	0.001	11.90×10
Wall	0.20	2.630×10^{3}	2.524×10^{2}	0.003	8.585×10
Conduction	0.40	1.965×10^{3}	2.066×10^{2}	0.01	5.864×10
	0.60	1.545×10^{3}	1.837×10^{2}	0.03	4.042×10
	0.80	1.254×10^{3}	1.678×10^{2}	0.07	3.025×10
	0.90	1.042×10^{3}	1.546×10^{2}	0.13	2.558×10
	0.96	——	1.396×10^{2}	0.25	2.347×10
	0.999			0.40	2.209×10
	1.000			0.65	2.144×10
				0.90	1.867×10
				0.999	
q_w		1×10^{4}	1×10^{3}		
$\frac{q_w}{k t_o}$		2.126×10^{3}	3.150×10^{2}		
t_o		2.126×10^{3}	3.150×10^{2}	q_w	1×10^{2}
t_{ad}/t_o		1.0	1.0	$\frac{q_w}{k t_o}$	46.05
Nu_x		2.352	1.587	t_o	46.05
				t_{ad}/t_o	1.0
				Nu_x	1.086

TABLE II — SUMMARY OF RESULTS

UNIFORM q_v, LINEAR VARIABLE WALL TEMPERATURE

Variable	Run / x/L	4	5	6	7	8	9	10	11	12
	0	1.000	1.000	1.000	1.000	1.000	1.000	1.000	1.000	1.000
	0.001	0.8746	0.8660	0.8630	0.7956	0.7831	0.7787	0.6650	0.6443	0.6377
	0.01	0.7964	0.7909	0.7896	0.6646	0.6572	0.6556	0.4293	0.4179	0.4159
	0.05	0.7021	0.7075	0.7114	0.5025	0.5146	0.5224	0.0849	0.1294	0.1526
	0.20	0.5937	0.6284	0.6662	0.3153	0.3841	0.4176	-0.3461	-0.0973	0
β	0.40	0.5425	0.6051	0.6348	0.2437	0.3610	0.4123	-0.2926	-0.0096	0.0669
	0.60	0.5243	0.6037	0.6390	0.2407	0.3703	0.4239	-0.2184	-0.0156	0.0609
	0.80	0.5284	0.6139	0.6520	0.2798	0.3947	0.4456	-0.1032	0.0444	0.1090
	0.90	0.5476	0.6259	0.6653	0.3294	0.4185	0.4665	-0.0026	0.0830	0.1399
	0.96	0.5730	0.6351	0.6776	0.3832	0.4398	0.4866	0.1009	0.1268	0.1763
	0.999	0.6173	0.6243	0.6750	0.5021	0.4455	0.4908	0.2803	0.1724	0.2150
	1.000	1.000	1.000	1.000	1.000	1.000	1.000	1.0000	1.000	1.000
	0	1.514×10^{3}	10.70×10^{2}	9.523×10^{2}	2.283×10^{2}	1.680×10^{2}	1.513×10^{2}	3.620×10	2.675×10	2.440×10
	0.001	1.479×10^{3}	10.65×10^{2}	9.496×10^{2}	2.234×10^{2}	1.672×10^{2}	1.509×10^{2}	3.538×10	2.664×10	2.434×10
	0.01	1.420×10^{3}	10.58×10^{2}	9.445×10^{2}	2.156×10^{2}	1.658×10^{2}	1.502×10^{2}	3.421×10	2.648×10	2.436×10
	0.05	1.342×10^{3}	10.40×10^{2}	9.362×10^{2}	2.058×10^{2}	1.639×10^{2}	1.492×10^{2}	3.311×10	2.629×10	2.414×10
	0.20	1.220×10^{3}	10.10×10^{2}	9.188×10^{2}	1.916×10^{2}	1.602×10^{2}	1.470×10^{2}	3.183×10	2.594×10	2.391×10
t	0.40	1.106×10^{3}	9.708×10^{2}	8.966×10^{2}	1.782×10^{2}	1.559×10^{2}	1.440×10^{2}	3.041×10	2.545×10	2.354×10
	0.60	0.986×10^{3}	9.302×10^{2}	8.686×10^{2}	1.632×10^{2}	1.497×10^{2}	1.396×10^{2}	2.835×10	2.462×10	2.294×10
	0.80	0.811×10^{3}	8.424×10^{2}	7.983×10^{2}	1.386×10^{2}	1.371×10^{2}	1.303×10^{2}	2.467×10	2.296×10	2.170×10
	0.90	0.672×10^{3}	7.566×10^{2}	7.282×10^{2}	1.170×10^{2}	1.244×10^{2}	1.204×10^{2}	2.128×10	2.121×10	2.036×10
	0.96	0.528×10^{3}	6.474×10^{2}	6.263×10^{2}	0.925×10^{2}	1.078×10^{2}	1.061×10^{2}	1.746×10	1.892×10	1.845×10
	0.999	0.218×10^{3}	4.359×10^{2}	2.518×10^{2}	0.453×10^{2}	0.734×10^{2}	0.584×10^{2}	1.116×10	1.425×10	1.267×10
	1.000	0	0	0	0	0	0	0	0	0
	0	23.878×10^{3}	15.937×10^{3}	13.880×10^{3}	22.098×10^{2}	15.453×10^{2}	13.659×10^{2}	21.363×10	15.012×10	13.456×10
	0.001	8.814×10^{3}	6.179×10^{3}	5.452×10^{3}	8.133×10^{2}	5.951×10^{2}	5.325×10^{2}	7.682×10	5.665×10	5.136×10
	0.01	5.508×10^{3}	4.176×10^{3}	3.770×10^{3}	5.059×10^{2}	3.982×10^{2}	3.643×10^{2}	4.531×10	3.632×10	3.381×10
	0.05	3.638×10^{3}	3.056×10^{3}	2.888×10^{3}	3.361×10^{2}	2.943×10^{2}	2.794×10^{2}	2.873×10	2.654×10	2.601×10
WALL	0.20	2.693×10^{3}	2.591×10^{3}	2.525×10^{3}	2.566×10^{2}	2.519×10^{2}	2.487×10^{2}	2.359×10	2.439×10	2.455×10
CONDUCTION	0.40	2.242×10^{3}	2.409×10^{3}	2.425×10^{3}	2.253×10^{2}	2.408×10^{2}	2.437×10^{2}	2.340×10	2.472×10	2.483×10
	0.60	1.897×10^{3}	2.265×10^{3}	2.346×10^{3}	2.040×10^{2}	2.322×10^{2}	2.388×10^{2}	2.284×10	2.414×10	2.440×10
	0.80	1.604×10^{3}	2.103×10^{3}	2.236×10^{3}	1.837×10^{2}	2.204×10^{2}	2.305×10^{2}	2.187×10	2.359×10	2.402×10
	0.90	1.364×10^{3}	1.900×10^{3}	2.062×10^{3}	1.632×10^{2}	2.033×10^{2}	2.163×10^{2}	2.037×10	2.242×10	2.305×10
	0.96	1.044×10^{3}	1.463×10^{3}	1.357×10^{3}	1.261×10^{2}	1.626×10^{2}	1.608×10^{2}	1.768×10	1.980×10	1.934×10
	0.999									
	1.000									
q_v		1×10^{4}	1×10^{4}	1×10^{4}	1×10^{3}	1×10^{3}	1×10^{3}	1×10^{2}	1×10^{2}	1×10^{2}
qt_0		5.044×10^{3}	26.07×10^{3}	499.5×10^{2}	8.083×10^{2}	42.00×10^{2}	79.913×10^{2}	102.8	660.35	1210.1
t_0		1.514×10^{3}	1.070×10^{3}	9.523×10^{2}	2.283×10^{2}	1.68×10^{2}	1.513×10^{2}	36.2	26.75	24.4
t_{to}/t_o		3.33	24.40	52.4	3.54	25.0	52.8	2.84	24.68	49.59
Nu		0.991	0.192	0.100	0.618	0.119	0.063	0.486	0.076	0.041

REFERENCES

1. Hammitt, F.G., "Modified Boundary Layer Type Solution for Free Convection Flow in Vertical Closed Tube with Arbitrarily Distributed Internal Heat Source and Wall Temperature," ASME Paper No. 57-81.

2. Hammitt, F.G., "Heat and Mass Transfer in Closed, Vertical, Cylindrical Vessels with Internal Heat Sources for Homogeneous Nuclear Reactors," Doctoral Thesis, Nuclear Engineering, University of Michigan, Feb. 1958.

3. Lighthill, M.J. "Theoretical Considerations on Free Convection in Tubes," Quarterly Journal of Mechanics and Applied Mathematics, Vol. 6, 1953, pp. 398-439.

4. Ostrach, Simon, and Thornton, P.R., "On the Stagnation of Natural-Convection Flows in Closed-End Tubes," ASME Paper No. 57-SA-2.

5. Murgatroyd, W., "Thermal Convection in a Long Cell Containing a Heat Generating Fluid," Atomic Energy Research Establishment, ED/R 1559, Harwell, England, 1954.

6. Martin, B.W., "Free Convection in an Open Thermosyphen, with Special Reference to Turbulent Flow," Proc. Royal Society, Series A, Vol. 230, 1955, pp. 502-530.

7. Haas, P.A., and Langsdon, J.K., "HRP-CP Heat Removal from a Proposed Hydroclone Underflow Pot Geometry for a Volume Heat Source," CF-55-10-7, Oak Ridge National Laboratory, October 5, 1955.